DOI: 10.1002/anie.200907091

Materials Science

Responsive Photonic Crystals

*Jianping Ge and Yadong Yin**

Keywords:
display technology · nanostructures · responsive photonic crystals · self-assembly · sensors

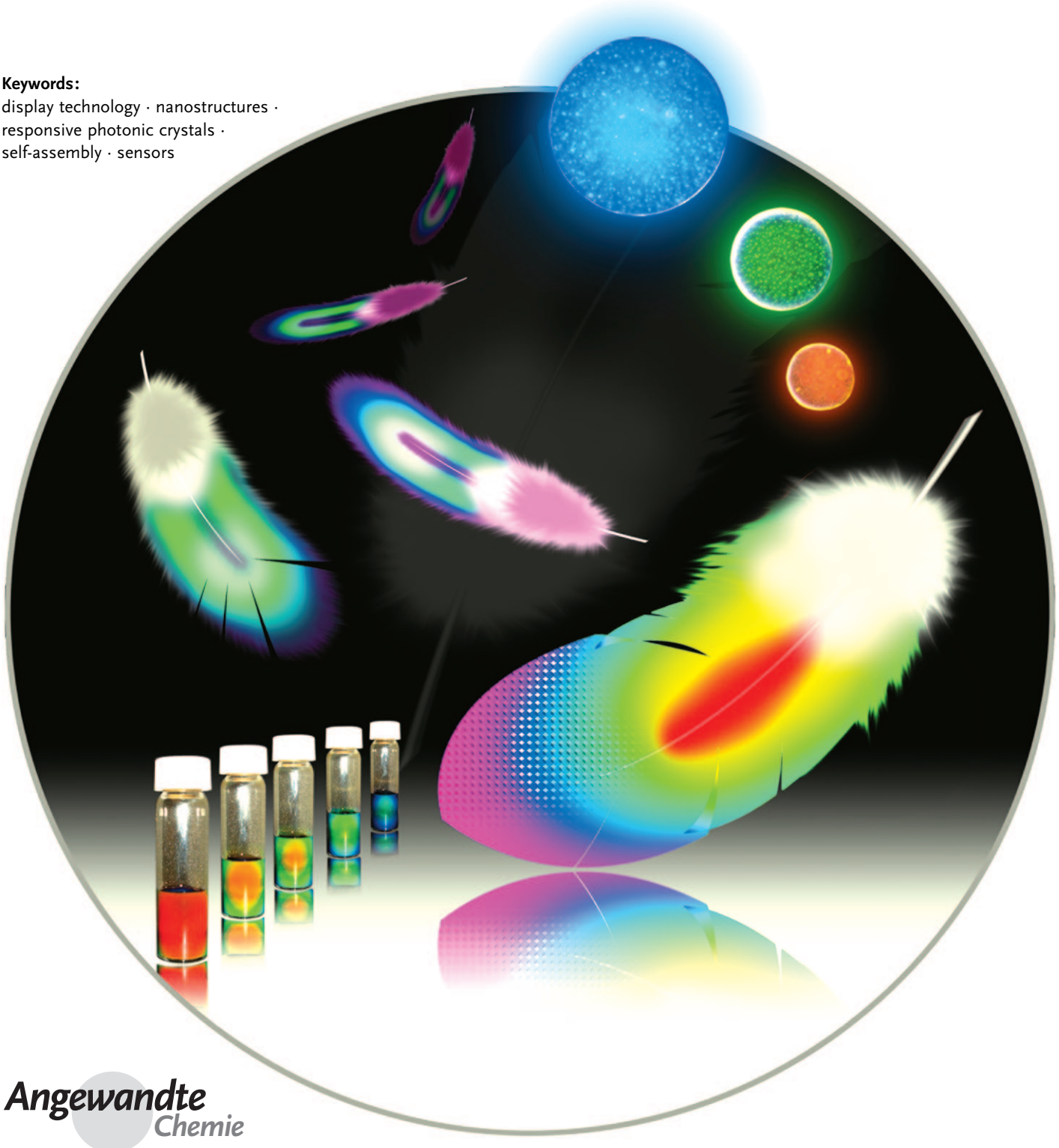

This Review summarizes recent developments in the field of responsive photonic crystal structures, including principles for design and fabrication and many strategies for applications, for example as optical switches or chemical and biological sensors. A number of fabrication methods are now available to realize responsive photonic structures, the majority of which rely on self-assembly processes to achieve ordering. Compared with microfabrication techniques, self-assembly approaches have lower processing costs and higher production efficiency, however, major efforts are still needed to further develop such approaches. In fact, some emerging techniques such as spin coating, magnetic assembly, and flow-induced self-assembly have already shown great promise in overcoming current challenges. When designing new systems with improved performance, it is always helpful to bear in mind the lessons learnt from natural photonic structures.

From the Contents

1. Introduction

The periodic modulation of the refractive index in a dielectric material creates a forbidden gap in the photonic band structure that excludes the existence of optical modes within a specific range of frequencies. Such photonic bandgap materials, more commonly known as photonic crystals, are attractive optical materials for controlling and manipulating the flow of light: they can be used as reflective coatings on lenses, color pigments in paints and inks, waveguides for directing the propagation of light along a specific path, highly reflective mirrors in laser cavities, and many other optical components.[1–6] In the past two decades, a number of methods have been developed to fabricate photonic crystals at various length scales. Notable examples include layer-by-layer stacking techniques using microfabrication tools,[7–9] electrochemical etching,[10,11] laser-beam-scanning chemical vapor deposition,[12] and holographic lithography.[13,14] The use of these methods for the fabrication of photonic crystals that can operate in the visible spectrum has remained a difficult task, as this task requires the periodicity of the structures to be on the same length scale as half the wavelength of the visible light, that is, approximately 400/2 nm (blue) to 700/2 nm (red). The fabrication challenges have provided a major driving force for the study of alternative approaches to photonic crystal preparation, such as the self-assembly of monodisperse colloidal particles, which can be performed under ambient pressure and temperature.[15–18] In this case, the periodic modulation of the dielectric constant is realized by self-assembling monodisperse colloidal objects such as silica (SiO_2) or polystyrene (PS) microspheres into ordered arrays. The resulting photonic properties are determined by the symmetry and lattice constant of the crystal and by the refractive index contrast between the colloids and the surrounding medium. The sizes of colloids are typically in the range of 100 nm to 1 μm so that a band gap in the visible region can be easily achieved in colloidal crystals. Although three-dimensional structures have been the focus of research owing to their important applications in photonic crystals,[19–22] lower-dimensional (one- and two-dimensional) periodic structures can also be fabricated by careful selection of the assembly conditions.[23,24] Besides colloidal crystals, well-defined block copolymers may also self-assemble into periodic photonic structures as driven by the phase separation of chemically different polymer blocks.[25,26]

There is a strong demand for photonic materials with properties that can be tuned by external stimuli. These responsive photonic crystals (RPCs) have important applications in areas such as color displays, biological and chemical sensors, inks and paints, and many optically active components. For example, tunable photonic crystals may be used in the future as optical switches for the full automation of optical circuits when significant improvements towards the quality of colloidal crystals and their response time are realized. Military vehicles covered with such materials may be able to dynamically change their colors and patterns to match their surroundings. Such materials might also be embedded in banknotes or other security documents for antifraud purposes. The hidden information cannot be revealed until an external stimulus such as a pressure or temperature change is applied. The photonic effect can also be used as a mechanism to develop chemical and biological sensors for detecting target analytes by outputting optical signals. These types of crystals may also find great use as active color units in the fabrication of flexible display media, including both active video displays and rewritable paper that can be reused many times. Currently, rewritable electronic paper is designed on the basis of E-ink technology,[27,28] in which switchable contrast is achieved by the electrophoresis of highly scattering

[*] Dr. J. Ge, Prof. Y. Yin
Department of Chemistry, University of California
Riverside, CA 92521 (USA)
Fax: (+1) 951-827-4713
E-mail: yadong.yin@ucr.edu
Dr. J. Ge
Department of Chemistry, Tongji University
Shanghai (China)

or absorbing microparticles sandwiched as a suspension between two panels of electrodes. Despite being lightweight and energy saving, such rewritable devices have met great challenges in producing color images owing to the fact that only bichromal states can be switched using the electric field. The incorporation of tunable photonic crystals might potentially provide a solution to this challenge.

Compared to microfabricated photonic crystals, self-assembled photonic crystals, in particular colloidal crystals, can be produced at much lower costs and with higher efficiencies owing to the parallel nature of the self-assembly processes. It is also more convenient to modify the building blocks before or after the formation of crystal structures to enable responsiveness to a given stimulus. As a result, the majority of research on RPCs has been focused on incorporating stimulus-responsive materials into the self-assembled photonic crystal structures. In principle, the stimulus can be any means that effectively induces a change in the refractive indices of the building blocks or the surrounding matrix and change in the lattice constants or spatial symmetry of the crystalline arrays. For example, oxide materials such as WO_3, VO_2, and $BaTiO_3$ have been used as matrix materials for producing tunable photonic crystals, because the refractive indices of these materials are sensitive to electric fields or temperature changes.[29–31] Colloidal arrays infiltrated with liquid crystals (LC) also show tunable photonic properties upon the application of an external electric field or exposure to a change in temperature.[32–34] Many approaches to tunable photonic crystals, on the other hand, are designed to control the lattice constant or the spatial symmetry of the crystals by the application of chemical stimuli, temperature variation, mechanical forces, electrical or magnetic fields, or light.[35–43] A notable example is a hydrogel/colloidal array composite in which the lattice spacing can be tuned by the swelling and deswelling of the hydrogel in a solvent such as water.[44] Depending on the specific applications, the challenges in developing responsive photonic crystals include limited tunability of the band gap, a slow response to external stimuli, incomplete reversibility, and difficulty of integration into existing photonic devices. The narrow tuning range is mainly due to the limited changes in the crystal structure or refractive index that the external stimuli can induce. The slow response is usually the result of retarded physical or chemical changes that the external stimuli may cause. Thanks to the high flexibility of the self-assembly processes, new building blocks and novel tuning mechanisms have been continuously developed in the past two decades, making colloidal RPCs an exciting line of research with many promising practical applications.

In this Review we will discuss recent developments in self-assembled photonic crystal structures whose photonic properties can be tuned in response to external stimuli. The objectives of this review are 1) to briefly summarize the fabrication of photonic crystal structures through self-assembly approaches; 2) to discuss general strategies for creating responsive photonic structures; 3) to give an overview of the various approaches for producing RPC structures with an emphasis on new developments in the field; and 4) to highlight a number of intriguing applications based on the stimulus-responsive photonic properties.

2. Formation of Photonic Crystals

Although the term "photonic crystal" was invented a little more than two decades ago, relevant studies have been carried out in one form or another for more than 100 years. For example, Newton and Hooke studied the color effects that can be seen in butterfly wings, beetle shells, and bird feathers. Such color effects, now often called structural colors, have been found to result from the interaction of light with periodically arranged microstructures of a single biological material.[45–49] Another natural photonic crystal is the precious opal, in which brilliant colors result from close-packed domains of colloidal spheres of amorphous silica, which were produced in highly siliceous pools and assembled into highly ordered arrays after years of sedimentation and compression under hydrostatic and gravitational forces.

Studies on the fabrication of artificial photonic crystals started intensively after the publication of two milestone papers in 1987 by John and Yablonovitch.[1,2] The fabrication methods can be roughly classified into two groups: top-down and bottom-up approaches. The top-down approaches often use traditional microfabrication methods, such as photolithography and etching techniques, to produce microstructures with desired shape, size, and order from bulk materials.

Jianping Ge received his BS and PhD in Chemistry from Tsinghua University in China in 2002 and 2006, respectively. He then spent three years at the University of California, Riverside to carry out his postdoctoral research. In 2009, he joined the Department of Chemistry at Tongji University as a professor. His research interests include the synthesis, self-assembly, and functionalization of magnetic nanostructures.

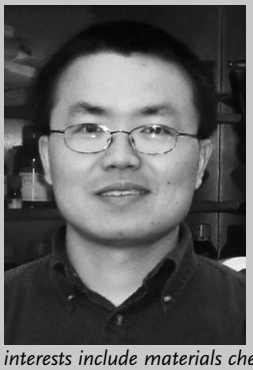

Yadong Yin obtained his BS (1996) and MS (1998) in Chemistry from the University of Science and Technology of China, and then received his PhD in Materials Science and Engineering from the University of Washington in 2002. He then worked as a postdoctoral fellow at the University of California, Berkeley, and the Lawrence Berkeley National Laboratory (LBNL). After serving as a staff scientist at LBNL for one year, he joined the Department of Chemistry at the University of California, Riverside as an assistant professor in 2006. His research interests include materials chemistry, surface and colloidal chemistry, and self-assembly processes, with a focus particularly on nanostructured materials and their photonic, bioanalytical, and catalytic applications.

Borrowed from the semiconductor industry, these methods have been successful in producing two-dimensional photonic crystals in semiconductor materials.[50–53] The microfabrication of 3D photonic crystals has proceeded more slowly than that of their 2D counterparts because of the dramatically increased cumbersomeness and complexity of the fabrication procedures. Attempts have been successfully made, however, to fabricate 3D photonic crystals such as the well-known "woodpile" structures constructed on a planar layer-by-layer basis.[7–9,54] Some unconventional microfabrication approaches have also been developed recently, including holographic lithography[55] and glancing-angle "spiral" deposition.[56] As microfabricated crystals are not typically used in the fabrication of responsive photonic structures owing to their high cost and low efficiency in production, we limit our discussion herein to the more relevant bottom-up approaches.

Bottom-up approaches generally involve the self-assembly of preformed building blocks into periodic photonic structures. The building blocks can be molecular species such as block copolymers or nanoscale objects such as SiO_2 or PS beads. Well-defined block copolymers can self-assemble into equilibrium phases consisting of one-, two-, and three-dimensional periodic photonic structures, depending on the composition and architecture of block copolymer macromolecules.[25,26] In this case, the self-assembly process is in fact a phase segregation process driven by the positive free energy of mixing of the chemically different polymer blocks. The simplest periodic structure consists of 1D alternating layers of different polymer blocks, while more complex structures, such as hexagonally packed cylinders and double-gyroid microdomain structures, can also form.[57,58] The periodic dielectric structures typically have mesoscopic length scales (10–100 nm) depending on the overall molecular weight. One challenge of the block copolymer photonic crystal systems is the small intrinsic dielectric contrast between typical copolymer microdomains, which makes it difficult to obtain large photonic band gaps in such materials. Fink et al. proposed a number of ways to enhance the dielectric contrast between the microdomains, for example by preferentially doping optically transparent nanocrystals with high dielectric constants into one or more of the block copolymer microdomains.[25]

Sub-micrometer colloidal spheres are the most favorable building blocks for the self-assembly of photonic crystals because they can be readily synthesized as monodisperse samples.[15,59] Typical materials include SiO_2 synthesized through sol–gel process and PS produced by emulsion polymerization, while other oxides (such as ZnO and TiO_2) and polymers (such as poly(methyl methacrylate), PMMA) can also be made into uniform spheres using similar methods.[60–62] The properties of colloidal spheres can be further modified by coating them with a shell of a different chemical composition in varying thicknesses. When coating is performed uniformly, the resulting core–shell colloids can maintain their narrow size distribution. By controlling the structure, size, and composition of the shells, the optical, electrical, thermal, and catalytic properties of the spheres can be tuned over a broad range. The coating strategy is also frequently used to tune the interactions between colloidal spheres and to stabilize dispersions of these spheres in a given medium.[63–65]

Colloidal spheres can be assembled into 1D, 2D, and 3D periodic structures. The assembly of colloids into 1D arrays mainly relies on physical templates. Xia et al. developed a strategy that combines physical templating and capillary force to assemble monodispersed spherical colloids into 1D chains.[23,66] When a colloidal dispersion is allowed to dewet from a solid surface that has been lithographically patterned with channels, the particles are trapped by the recessed regions and assembled into 1D chains. Recently, we also reported the formation of 1D particle chains by self-assembly of superparamagnetic colloids using external magnetic fields.[67,68]

The commonly used strategies to self-assemble monodispersed spherical colloids into ordered 2D arrays are based on the lateral capillary interaction, which originates from the deformation of the liquid surface.[69–72] The colloidal particles are typically assembled at the air–liquid interface or in a thin liquid layer supported on a flat solid substrate.[73–78] The arrays assembled on the surface of a liquid can be subsequently transferred onto various solid substrates if needed. When the assembly is performed on substrates, their surfaces must be flat, clean, and chemically homogeneous in order to generate a high-quality array with relatively large domain sizes of greater than hundreds of micrometers. Spin coating can be used to assist the assembly of colloids on a solid substrate.[79] Interestingly, by controlling the acceleration of the spin, it has been possible to produce high-quality wafer-scale 2D non-close-packed colloidal arrays.[80,81] An alternative method to create 2D arrays is electrophoretic deposition, which uses a strong electric field to assemble colloidal dispersions confined between two parallel solid electrodes.[82–84]

With some modification, the methods used for 2D assembly can be employed to construct 3D crystals. Colvin et al. have demonstrated that lateral attractive capillary forces can be used to build 3D lattices with well-controlled numbers of layers.[85] The electrophoretic deposition method has been further extended by López and co-workers to organize silica colloids into 3D opaline structures.[86] To achieve a high degree of order and large domain sizes, several other methods have also been widely used for the assembly of 3D crystals, including those that use sedimentation, repulsive electrostatic interactions, and physical confinement to assemble monodispersed colloids. Sedimentation in a gravitational field seems to be the simplest approach for building 3D crystals.[19] While it can be carried out using simple setups, this method in fact involves several complex processes such as gravitational settling, Brownian motion, and crystallization (nucleation and growth). A number of parameters must be carefully chosen to grow highly ordered colloidal crystals with a large domain size, including the size, uniformity, and density of the colloids, as well as the rate of sedimentation. Sedimentation is particularly useful for assembling silica colloids owing to the relatively high density of amorphous silica.[87–91] The main disadvantages of this method include the poor control over the morphology of the top surface and the thickness of the crystalline arrays, the long preparation time, and the polycrystalline nature of the products.

Highly charged spherical colloids suspended in a dispersion medium can spontaneously self-organize into crystalline structures, driven by the minimization of electrostatic repulsive interactions.[21,22,92–94] When the volume fraction of colloids is so high that the electrostatic screening length is larger than the average center-to-center distance, the colloids strongly repel each other and crystallize into ordered structures.[95–97] The colloidal crystals prepared using this method are typically non-close-packed, because the repulsive electrostatic interactions keep the particles away from each other. While this method has very strict requirements regarding the experimental conditions such as the surface charge density, the colloidal concentration, and the ionic strength, it represents the most powerful and successful route to relatively large-scale 3D crystals of up to several centimeters.

It has been reported that monodispersed colloids often self-assemble into long-range-ordered lattices when they are subjected to a physical confinement provided, for example, by a pair of parallel substrates.[98–100] On the basis of this observation, Xia et al. demonstrated an effective approach that allowed for the fabrication of colloidal crystals with domain sizes as large as several square centimeters by using a specially designed packing cell.[101–103] A key to the success of this method is the continuous sonication, under which each particle in the colloid is placed at the lattice site that represents a thermodynamic minimum. This method is relatively fast, and it also provides tight control over the surface morphology and the number of layers of the crystalline assemblies.

3. General Strategies To Create Responsive Photonic Structures

Responsive photonic crystals are materials with photonic band-gap properties that can be tuned by external stimuli. To create such materials, a stimulus-response mechanism needs to be coupled with the photonic crystal structure. A crucial question is then what will cause changes in the band gap of photonic crystals. To answer this question, it is necessary to briefly introduce the physical principles behind the photonic structures.

The diffraction properties of periodic arrays can be described by Bragg's law. Here we first use a Bragg stack, also called Bragg reflector or Bragg mirror, as a simple example of photonic crystals to reveal how the photonic properties are affected by the parameters of the crystal structures. Bragg stacks typically consist of alternating layers of high- and low-refractive-index materials. They have been extensively studied and were widely used even before the term "photonic crystal" was invented because of their high reflectivity, convenient fabrication process, and relatively easy prediction of their optical properties. The diffraction of a Bragg stack can be described by the Bragg–Snell law [Eq. (1)], which holds for normal incidence and non-absorbing materials:[104,105]

$$m\lambda = 2(n_l d_l + n_h d_h) \tag{1}$$

where m is the diffraction order, n_l and n_h are the refractive indices of the low- and high-refractive-index materials, and d_l and d_h are the respective thicknesses. The reflectivity R of the Bragg stack depends on the contrast of refractive index and the number of bilayers (N) comprising the stack [Eq. (2)]:

$$R = \left[\frac{n_0 - n_s(n_l/n_h)^{2N}}{n_0 + n_s(n_l/n_h)^{2N}}\right]^2 \tag{2}$$

where n_0 and n_s are the refractive indices of the surrounding medium and the substrate, respectively.[106] If we assume the central wavelength of the photonic band is λ_0, then it is also possible to calculate the bandwidth $\Delta\lambda_0$ of the photonic stop band [Eq. (3)]:

$$\Delta\lambda_0 = \frac{4\lambda_0}{\pi}\arcsin\left(\frac{n_h - n_l}{n_h + n_l}\right) \tag{3}$$

As seen from these equations, the photonic band-gap properties of the 1D system are determined by not only the properties of the individual components but also the architecture of the stack and the properties of the surroundings. For example, increasing the refractive index contrast between the materials in the Bragg pairs increases both the reflectivity and the bandwidth, and increasing the thickness of the layers increases the diffraction wavelength. If a stimulus can induce changes in any of these parameters, corresponding changes in the photonic properties can be expected. A responsive photonic crystal can be realized when the changes in photonic properties are reversible. In fact, as will be described in more detail later (Section 4.2.2), many 1D responsive photonic crystals have been designed on the basis of the reversible changes in the thickness or refractive index of the dielectric layers.[106,107] In addition to changing the parameters of Bragg diffraction, the periodic structure can also be disrupted by incorporating a defect layer with distinct optical thickness, thus creating allowed photonic states for a certain range of previously forbidden energies.[108] In this case, tunable photonic properties can be achieved by simply making the defect layer responsive to external stimuli.

Similar analyses can be applied to more complex systems such as 3D colloidal photonic crystals.[109] To simplify the discussion, we focus herein on the factors that control the diffraction wavelength. A 3D colloidal crystal diffracts light of a specific wavelength as determined by Bragg's law [Eq. (4)]:

$$m\lambda = 2nd\sin\theta \tag{4}$$

where m is the order of diffraction, λ is the wavelength of incident light, n is the mean refractive index of the system composed of colloids and voids, d is the spacing between the planes in lattice, and θ is the glancing angle between the incident light and diffraction crystal planes.[97,110] Under practical conditions, the colloidal spheres are embedded in matrix materials such as solvents and polymers, and Bragg's law can be approximately expressed as in Equation (5) by considering the effective index of the system:

$$m\lambda = \sqrt{\frac{8}{3}}D\left(\sum_i n_i^2 V_i - \sin^2\phi\right)^{1/2} \quad (5)$$

where D is the center-to-center distance between nearest spheres, n_i and V_i are, respectively, the refractive index and volume fraction of each component, and ϕ is the angle between the incident light and the sample normal.[111]

These equations provide guidelines for designing responsive photonic crystals. In principle, stimulus-responsive changes in any parameter that appears in the Bragg equation and contributes to the determination of the diffraction wavelength can be employed for the creation of RPCs. We can summarize the parameters that can be tuned to affect the properties of photonic crystals (Figure 1): 1) The lattice

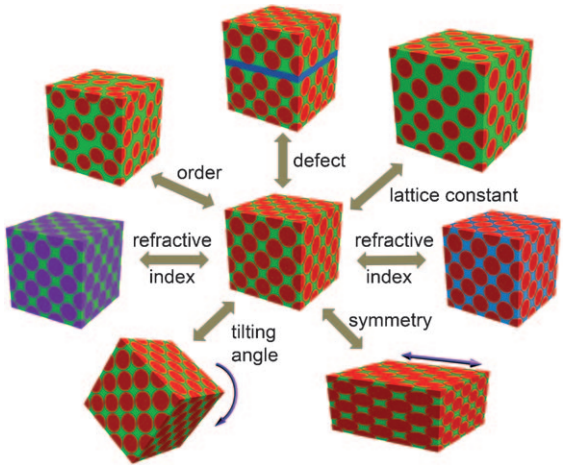

Figure 1. Schematic illustration of the parameters that can be tuned in a 3D responsive photonic crystal structure.

constant of the crystals, including the interparticle distance in 3D systems and layer thickness in 1D Bragg stacks, is the parameter that has been most extensively used to tune photonic properties. For 1D systems, the dielectric layers need to be composed of materials that display expansion/contraction properties. For 3D systems, the colloidal crystals can be embedded in a polymer matrix that can expand or contract, such as hydrogel and elastic polymers. The lattice constant and consequently the diffraction of RPCs can be modulated by applying various stimuli, such as mechanical deformation, hydrogel swelling and deswelling, thermally induced polymer volume or phase transition, and charge-induced expansion and contraction. A very important system in this category involves 3D colloidal crystals that are embedded in a responsive hydrogel matrix. The as-formed composite opal structures show tunable diffraction when they are subjected to solvent swelling or deswelling, with the diffraction wavelength dependent on the degree of swelling of the hydrogel, as given in Equation (6):[112]

$$m\lambda = \sqrt{\frac{8}{3}}D(d/d_0)\left(\sum_i n_i^2 V_i - \sin^2\phi\right)^{1/2} \quad (6)$$

Here, d and d_0 denote the sizes of the gel in the equilibrium state at a specific condition and in the reference state. 2) The change in crystal structure has a dramatic effect on the photonic properties owing to the changes in interplanar spacing and the sphere density on the diffracting planes. It is worth noting that in many cases, such as mechanical stretching of crystals embedded in elastomers, the change in lattice constant is anisotropic, which results in a change in the symmetry of crystals. 3) Changing the effective refractive index is also an important strategy for designing RPCs. Generally, the change in refractive index is accompanied by phase-transition processes or the introduction of new substances, for example by selective or nonselective absorption or infiltration of solvents and gas molecules, high-temperature phase transition, optically induced chromophore phase transition, and electrically induced liquid-crystal-molecule reorientation. It has also been reported that high-intensity illumination of a colloidal crystal made of optically nonlinear materials may rapidly heat the colloidal particles and decrease their refractive index.[113,114] 4) The photonic properties can be effectively tuned by changing the relative orientation of a photonic crystal when the direction of incident light is fixed. The photonic crystals must possess anisotropic structures or properties that allow them to rotate in a controllable manner in response to external stimuli, for example an electric or magnetic field. The orientation tuning has mostly been demonstrated in systems composed of magnetically anisotropic structures. 5) Defects with responsive properties can be introduced into photonic crystal structures to enable tunability of photonic properties. For example, RPCs can be constructed by sandwiching a layer of liquid crystals or other responsive polymers in Bragg stacks. The variation in thickness or refractive index induced by different stimuli can change the location of the allowed state in the original forbidden gap. As many materials with various responsive behaviors can be introduced into a crystal as the defect layer, this method significantly enhances the diversity of tools for the manipulation of photonic properties. 6) In some cases, the degree of order in photonic structures can be controlled by applying external stimuli, such as optical illumination or magnetic fields, so that the diffraction intensity can be switched on and off reversibly. In the sections below, the working mechanisms, tuning methods, and applications of various RPCs designed by following these strategies will be systematically discussed.

4. Responsive Photonic Crystals

Responsive photonic crystals are dielectrically periodical structures, that can alter their diffraction wavelength or intensities upon exposure to physical or chemical stimuli. In addition to the periodic structures that are required for traditional photonic crystals, a stimulus-responsive material has to be incorporated into the system. There are generally two approaches to introduce such responsive materials. In the first case, the responsive materials are directly prepared in the form of building blocks that can be used for constructing photonic crystals. A typical example is the 1D Bragg stacks

formed by self-assembly of block copolymers that contain segments that can expand when exposed to certain solvents. In the second case, the periodic structures are defined first, and then the responsive materials are filled into the interstitial space to form a composite material that is optically tunable and mechanically stable. If the responsive material cannot provide enough mechanical strength, an inverse opal structure will be formed by first infiltrating an inert material into the interstitial space of the periodic structure to form a robust framework and then removing the original periodic template through calcination or chemical etching. Finally, the responsive materials are filled into the porous structure of the inverse opals.

In both cases, the responsive materials can be chosen from a wide variety of substances that can initiate changes in the lattice constant, refractive index, orientation, and order of the crystal structures. They typically include polymers, inorganic solids, and some molecular species. The general procedure in the design and fabrication of RPCs includes the selection of responsive materials according to specific needs, incorporation of the responsive materials into photonic crystals, and optimization of the performance of the photonic system. A good RPC is usually characterized by a high response rate, reversible tuning, a large tuning range of the diffraction wavelength or intensity, and the possibility to be miniaturized for integration into existing devices.

4.1. Thermoresponsive Photonic Crystals

4.1.1. Thermal RPCs Based on Polymer Swelling

Polymer-based thermosensitive photonic crystals were probably the first successful example of RPCs that combine a functional and responsive polymer matrix with colloidal crystals. Since the pioneering work by Asher et al.,[97] a large number of RPCs have been developed that are similar in structure but sensitive to various stimuli. A classic system is composed of mesoscopically periodical materials that are created by embedding a non-close-packed colloidal crystal in a thermosensitive hydrogel of poly(*N*-isopropylacrylamide) (PNIPAM). PNIPAM is a thermosensitive polymer that undergoes a reversible volume phase transition between a hydrated state and a dehydrated state around its lower critical solution temperature (LCST, ca. 32 °C) in water. When the temperature increases, the polymer expels water and contracts so that the interparticle distance in the colloidal crystal decreases, leading to a blue shift in the diffraction. This hydrogel/colloidal crystal composite film shrinks and swells reversibly when the temperature is switched between 10 and 35 °C. The diffraction wavelength can correspondingly be tuned between 704 and 460 nm, which covers the entire visible range.

Interestingly, colloidal crystals assembled from pure hydrogel colloids did not show a significant wavelength change but instead had an intensity response to temperature.[97,115] A completely reversible order–disorder transition in response to large temperature fluctuations has been observed. Upon heating to above the LCST, the initially close-packed crystal cannot sustain its order owing the shrinkage of the hydrogel particle, and so the system becomes a disordered, free-flowing solution. An important feature of this system is that the iridescent crystal can reform spontaneously upon cooling. Hu et al. reported an improved system in which 2-hydroxyethyl acrylate modified PNIPAM colloids were assembled and then covalently linked through divinylsulfone.[116] The covalent linkages between the particles not only greatly enhance the thermal stability of the crystal structure but also effectively reduce the time for restoring the ordered structure at low temperature, thus making the hydrogel crystals more suitable for applications such as sensors and displays. It is believed that disturbed hydrogel particles in a cross-linked assembly are able to return to their equilibrium crystalline positions quickly through restoring forces provided by the network elasticity.

Takeoka and Watanabe further extended the synthesis of thermoresponsive composite films, originally developed by Asher et al., to the fabrication of a porous crystalline gel by templating against a close-packed silica colloidal crystal.[117,118] The porous gel was fabricated by polymerizing a solution mixture containing monomer, cross-linker, and initiator that was infiltrated into a preassembled silica colloidal crystal and then selectively removing the silica colloids by HF etching. Without the silica particles, the porous gel still showed a reversible photonic response to temperature change, thus suggesting that the voids left by the etching of silica still maintained a periodic arrangement (Figure 2). The cross-link density of the porous gel was found to be crucial to the tuning range of the photonic crystal, as gels with low degrees of cross-linking swelled more and led to a greater red shift in diffraction when the temperature decreased.

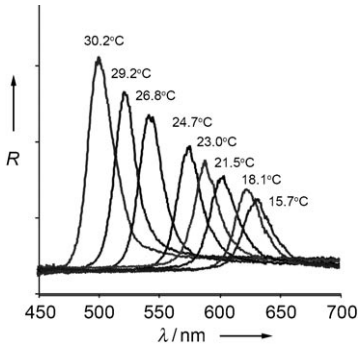

Figure 2. Temperature dependence of the reflection spectrum of porous NIPAM gel built with a colloidal crystal template composed of 210 nm silica particles. *R* = reflectance. From Ref. [117].

The synthetic strategy has been further developed to fabricate RPCs that can respond to dual stimuli.[119–121] For example, a porous gel made by copolymerization of *N*-isopropylacrylamide (NIPAM) and methacrylic acid (MAAc) displayed a response to variations not only in temperature but also in the pH value of the surrounding solution.[119] It has also been found that the porous P(NIPAM-*co*-MAAc) gel fixed on an anodic electrode exhibits an electrochemically triggered two-state switching between two arbitrary structural colors at a constant temperature.[120] The two-color switching can be

achieved reversibly in a few minutes, because the electrolysis of water causes a rapid decrease in the pH value in the vicinity of an anode and the gel no longer shrinks when the pH value decreases to 3.8. Similarly, a porous gel synthesized by copolymerization of NIPAM and 4-acryloylaminoazobenzene (AAB) showed continuous shifting in diffraction wavelength owing to the isotropic volume change upon heating and cooling. The P(NIPA-*co*-AAB) gel was also capable of switching its diffraction wavelength discontinuously between two equilibrium states upon irradiation with 366 and 450 nm light.[121] The light-triggered switching was caused by the change in the dipole moment of the azobenzene group attached to the polymer network, which affected the free energy of the mixing process between the polymer network and water molecules. As a result, the reversible change in the dipole moment of the azobenzene moiety induced a volume change in the gel that affected the photonic properties.

Besides the widely used colloidal crystals, the complexity of photonic crystal structures as well as the range of output photonic signals can be further extended by using beam lithographic techniques. Recently, Yang et al. employed prism holographic lithography to fabricate a 2-hydroxyethyl methacrylate (HEMA) based 3D hydrogel, the diffraction wavelength of which can be tuned in the near infrared range between 2200 and 1600 nm when the temperature is switched between 25 and 50 °C.[122] They also demonstrated the viscoelastic deformation of the system by capturing the morphology evolution using chemical vapor deposition of a thin film of silica on the hydrogel network.

4.1.2. Thermal RPCs Based on Phase Change of Inorganic Materials

Polymer-based thermal RPCs have intrinsic disadvantages that limit their application in some specific situations. For example, hydrogel-based RPCs cannot operate at high temperatures owing to their physical characteristics, and the switching rate of optical signals between two working states might become a major concern in applications where a fast response is required. Alternatively, inorganic materials with large changes in refractive index around their phase-transition points can be used to replace the thermoresponsive polymer matrix for a broader application range. Unlike the polymer-based RPCs, in which photonic tunability is limited by the sluggish volume change, the inorganic systems are usually based on the refractive-index change, which can be achieved at much higher rates. The inorganic-based RPCs, however, typically show a limited tuning range of the diffraction wavelength owing to the small changes in the refractive index as induced in the phase transitions of inorganic solids.

Xia et al. reported a thermally switchable photonic crystal fabricated by assembling core–shell particles comprising α-Se cores and Ag_2Se shells. The diffraction red-shifted from 1392 to 1497 nm as the temperature rose from 110 to 150 °C.[38] Such crystals presented a reversible stop band in response to temperature fluctuations around the phase transition temperature of Ag_2Se (133 °C), because the phase transition between semiconductive β-Ag_2Se and conductive α-Ag_2Se changed various physical properties, including the dielectric constant. Apart from Ag_2Se, other inorganic materials with phase-transition behaviors and significant changes in refractive index, such as $BaTiO_3$, VO_2, and Si, can also be used as active components for constructing thermal RPCs.[30,31,123] For instance, the phase transition as well as the stop band shift of a SiO_2/VO_2 RPC can be accomplished within 500 ps by laser-induced microannealing in a confined region, thus fully revealing the potential of the system as an optical switch in optoelectronic devices.[30] Ferroelectric crystalline $BaTiO_3$ has also been filled into SiO_2 colloid crystals by combining a sol–gel process and a thermal treatment.[31] The photonic band gap of the composite crystals exhibited a strong temperature dependence in the vicinity of the ferroelectric phase transition of $BaTiO_3$ (100–150 °C), which was attributed to the change of the refractive index of the $BaTiO_3$ around its Curie temperature.

4.2. Chemically Responsive Photonic Crystals

4.2.1. Chemical RPCs Based on Polymer Swelling and Shrinkage

Chemical RPCs are complex systems, as they cover the influence of various chemical species, including ions, solvent and vapor molecules, and biomolecules, upon the optical properties of photonic crystals. Based on the well-known volume change of many polymer hydrogels responding to changes in chemical environment, Asher et al. prepared the first ion-sensitive hydrogel photonic crystals by attaching a molecular-recognition group (crown ether) onto the polymer chains for the selective binding of certain metal ions, such as Pb^{2+}, Ba^{2+}, and K^+.[44,124,125] The binding between the crown ether and these cations localized the positive charge on the gel network and caused an increase of Donnan osmotic pressure within the gel owing to the introduction of mobile counterions to the bonded cations, thus leading to the swelling of the hydrogels and a red shift of the diffraction. Since the degree of swelling, and correspondingly the shift of diffraction peak, is related to the number of bonded charges, such RPCs are capable of detecting ions such as Pb^{2+} with concentrations ranging from 0.1 μM to 10 mM in a solution of moderate ionic strength. Similarly, 4-vinylbenzo-[18]crown-6[112] and 8-hydroxyquinoline[126] grafted hydrogels have been designed to sense K^+ and Cu^{2+} (also Ni^{2+}, Co^{2+}, and Zn^{2+}), respectively. Figure 3 displays the reflection spectra and photos of the porous gels responding to Na^+ and K^+ ions of different concentrations. Both systems show a red shift in diffraction as the ion concentration increases within the millimolar scale. But an exception should be noted: At extremely low concentrations (below 1 μM), the diffraction blue-shifts as concentration increases owing to the formation of complexes coordinated by two ligands, which thereby shrinks the gel driven by cross-linking.

As a special ion RPC, a pH-responsive photonic crystal detects the concentration of H^+, an important parameter for many water-based reactions and analyses. By combining the responsive materials with photonic crystal templates, Braun and Lee reported an inverse opal pH RPC based on a mesoporous hydrogel synthesized by polymerizing HEMA

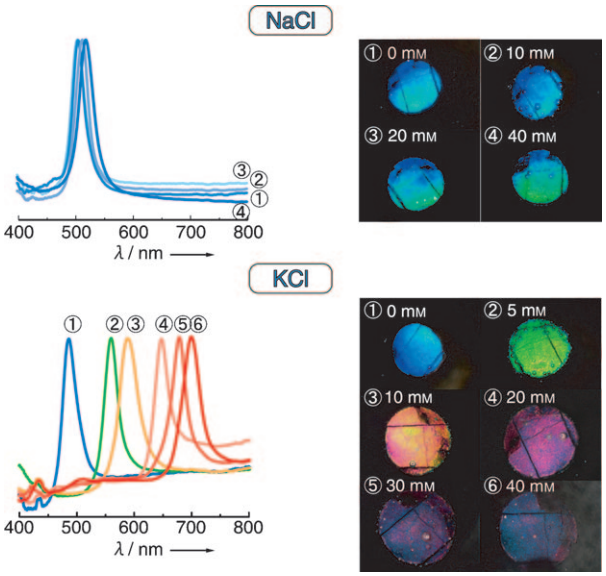

Figure 3. Reflection spectra and related photographs of periodically ordered interconnecting porous gels responding to sodium and pottasium ions of different concentrations. From Ref. [112].

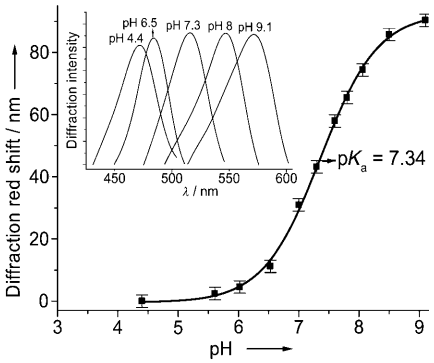

Figure 4. Response to pH value by a 2-nitrophenol-modified hydrogel/colloidal crystal composite film in aqueous solution containing 150 mM NaCl. The inset shows the changes in diffraction of the film as a function of pH value. From Ref. [128].

and acrylic acid (AA).[111] The as-designed RPC showed superior properties including facile diffusion, rapid response, and robust mechanical strength. As the pH value increased, the carboxy groups on the polymer backbone ionized to carboxylate anions, which resulted in an increasing Donnan osmotic pressure and correspondingly the swelling of the hydrogel and a shift in the Bragg diffraction. As the pH value was varied between 2 and 7, the pH RPC impregnated in a phosphate buffer solution showed an apparent hysteresis in diffraction wavelength between 544 and 850 nm. This effect can be explained by the kinetics of hydrogel expansion and contraction, which are delayed diffusion-limited processes with equilibration times of approximately 20 min.

A major interference in the detection of ions with a high concentration (millimolar scale) is ionic strength, as the increase of ionic strength in the solution will decrease the Donnan osmotic pressure, thus seriously shrinking the gel and eventually blocking its response to ions. Asher and Lee reported a polyacrylamide (PAAm) based pH RPC that showed a red shift of diffraction upon an increase in the pH value from 2.0 to 9.6 but a subsequent blue shift from pH 9.6 to 11 owing to the influence of ionic strength, which was estimated to be around 1 mM at pH 11.[127] Later, they improved the response of the pH RPC at high ionic strengths by attaching nitrophenol groups onto the PAAm backbone.[128,129] At higher pH values, the phenol groups dissociated to phenolates so that hydrogel swelling was enhanced owing to the larger solubility of phenolates in water, which compensated for the shrinkage at high ionic strength. As shown in Figure 4, the modified RPC showed a continuous shift in the Bragg diffraction wavelength from 470 to 590 nm as the pH value increased from 4.4 to 9.1 in an aqueous solution containing 150 mM NaCl.

In some special chemical environments, such chemical RPCs are even capable of outputting more complex optical responses. Recently, a porous poly(NIPAM-[Ru complex]) photonic gel has been reported to exhibit a self-sustaining peristaltic motion as well as periodical diffraction changes, completely synchronized with a nonlinear oscillatory Belousov–Zhabotinsky (BZ) reaction.[130,131] The porous poly(NIPAM-[Ru complex]) gel was prepared by the copolymerization of NIPAM and the ruthenium complex in the voids of a silica colloid crystal and subsequent template removal. As the ruthenium complex periodically changed its redox state during the BZ reaction, the polymer network cyclically swelled and deswelled because of the change in the osmotic pressure inside the gel. When the thickness of the gel was smaller than the wavelength of the chemical wave of the BZ reaction, a self-sustaining peristaltic motion was produced in the gel. The porous structure was designed to improve the swelling–deswelling response to the redox changes so that there would be no phase difference between the mechanical and chemical oscillation. Since the ruthenium-complex-based BZ reaction can be inhibited by bromide ions produced from visible light illumination, such wormlike motion can be completely stopped by a sufficiently strong light exposure (6.45 mW) and can also be quickly recovered once irradiation is withdrawn.

4.2.2. *Chemical RPC Based on Porous Structure and Refractive Index Tuning*

In addition to the introduction of recognition groups, changing the refractive index by infiltration of chemical species such as solvents and vapors into the porous photonic structure is also an effective method to tune the properties of the photonic crystals. Stein et al. reported the synthesis of ceramic macroporous inverse opal materials, such as silica, alumina, and zirconia, through sol–gel processing around the polymer template and subsequent template removal.[132] This photonic crystal was capable of distinguishing many solvents, including methanol, ethanol, 2-propanol, tetrahydrofuran, dimethylformamide, toluene, and 1,2-dibromoethane, as its diffraction red-shifted in high-refractive-index solvents. This effect can be well explained by Bragg's law and Snell's law. The shift of the stop band was more than three times greater

than those reported for opal structures owing to the porous structure and thereby larger changes in the refractive index n.[133] The response of this solvent RPC was precise and predictable, but the selectivity between two solvents with similar refractive indexes remained an unsolved problem.

According to this concept, the groups of Miguez and Ozin further shrunk the pore size and fabricated sol–gel-based mesoporous Bragg stacks (MBSs) composed of spin-coated multilayers of mesoporous TiO_2 and SiO_2, which showed higher sensitivity to low concentrations of molecules owing to the capillary condensation within the nanopores and better selectivity owing to their molecular sieve functions.[134,135] The difference in hydrophobicity of the two components (TiO_2 and SiO_2) further improved the selectivity when distinguishing alcohols and alkanes, such as *n*-hexane and 2-propanol, even though they have close refractive indices. By increasing the percentage of *meso*-SiO_2, a more hydrophobic component than *meso*-TiO_2, the affinity to *n*-hexane and thereby the swelling increased accordingly, thus suggesting that such MBS devices can be tailored by tuning the layer thickness, composition, and surface properties. Figure 5 a shows a typical

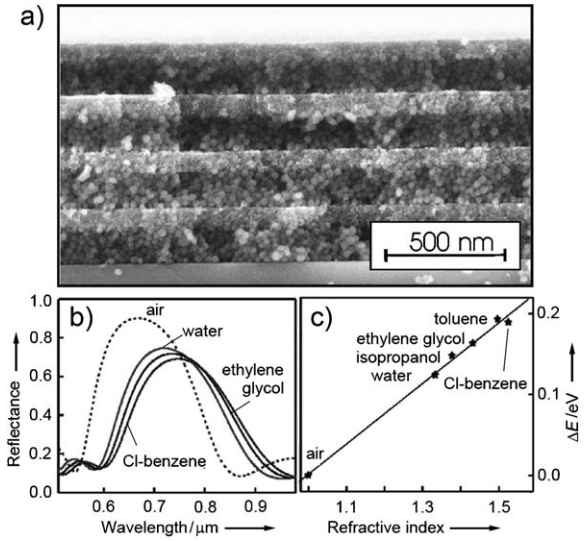

Figure 5. a) SEM image of the cross-section of an eight-layer Bragg reflector made of silica and titania nanoparticles deposited alternately on the substrate. b) Reflection of the Bragg reflector infiltrated with water, ethylene glycol, and chlorobenzene. c) Relationship between the Bragg peak position shift and the refractive index. From Ref. [136].

SEM image of the cross section of an eight-layer Bragg stack made of SiO_2 and TiO_2 nanoparticles deposited alternately on the substrate by spin-coating.[136,137] The specific color changes induced by the infiltration of solvents of different refractive indices makes these systems promising candidates to distinguish solvents such as water, ethylene glycol (EG), and chlorobenzene (Figure 5 b). As summarized in Figure 5 c, a linear relationship exists between the Bragg peak position shift and the refractive index of the solvents.

The introduction of porosity makes the Bragg stacks accessible to liquid as well as gaseous analytes.[106] TiO_2–SiO_2 MBSs prepared using a spin-coating method similar to that above have also been used to sense organic vapors.[136–138] In contrast to sol–gel films, the porosity of which is sensitive to aging conditions, MBSs fabricated using well-defined nanoparticles show reproducible porosity, controllable pore size (by choosing different sized particles), and no percolation of soluble precursor to the already deposited layer. The exchange of the gaseous nitrogen for organic vapors inside the porous multilayer stacks significantly influences the refractive index of the silica and titania layers, thus making the film capable of indicating the relative pressure of organic vapors, such as toluene, in nitrogen.[138] The fabrication strategy of such nanoparticle-based MBSs can be extended to other materials, in particular SnO_2, which is believed to be more suitable for gas sensing because of the possibility of combining both optical responses and changes in electrical conductivity.

Electrochemical etching has been widely used for the fabrication of porous silicon Bragg stacks.[139–141] Highly sensitive probes for organic vapors and biochemical interactions can be produced by combining different recognition modes with the optical responses. Chemical vapor deposition has also been used to directly synthesize chemical RPCs composed of alternating layers of titania and poly(2-hydroxyethyl methacrylate) (PHEMA).[142] The novel organic–inorganic hybrid Bragg mirror was found to be highly sensitive to water vapor (humidity) owing to the swelling of un-cross-linked PHEMA layers. The swelling does not affect the optical thickness of the high-refractive-index inorganic layers, which is analogous to the structural color-changing mechanism found in many natural species.

Natural photonic structures can also be employed as RPCs with responses to chemical species. The iridescent scales of the *Morpho sulkowskyi* butterfly were found to show a different optical response to different individual vapors, thus providing information about the nature and concentration of the vapors.[45] A range of closely related vapors (water, methanol, ethanol, and isomers of dichloroethylene) could be identified when they were analyzed individually. The response is believed to result from the combined action of two mechanisms: physical adsorption and capillary condensation of condensable vapors in the nanometer-sized domains of the *M. sulkowskyi* scales. By studying the mechanism of superior performance of the natural RPCs, Potyrailo et al. emphasized the importance of the combined effects of the surface properties of the structure and the properties of the detected vapors, such as surface tension, molar volume, and molecular shape and size of the vapors, in designing artificial RPC systems. They further pointed out that an enhancement of sensitivity of vapor response could possibly be achieved by formation of hierarchical substructures with higher surface areas and by tailoring surface properties of features with a given spatial periodicity.

4.3. Mechanically Responsive Photonic Crystals

Compared with stimuli involving temperature or chemicals, mechanical pressing or stretching represents a concep-

tually straightforward but effective strategy for controlling the properties of photonic crystal structures. To enable mechanical deformation, a continuous phase of elastic polymer is typically required. The mechanical RPCs are composite structures fabricated by infiltrating monomer or prepolymer into preassembled photonic crystal structures with subsequent thermo- or photopolymerization. If needed, the original crystal templates can be removed after polymerization. The maximum ratio of mechanical pressing or stretching is determined by the elastic properties of the polymer matrix. While stretching is possible for most elastic systems, mechanical RPCs that can change color by pressing are usually fabricated from crystal templates with non-close-packed structures. For composites composed of hydrogel and colloid crystals, the interparticle spacing can be 2.6 times greater than the particle size, which provides sufficient volume for compression of the lattice.

A composite film made of *N*-vinylpyrrolidone, acrylamide, and polystyrene colloids was reported by Asher et al. in 1994 to blue-shift its diffraction from 573 to 538 nm when stretched, as caused by the decrease in lattice spacing along the normal orientation of the film.[110] To improve the mechanical strength, poly(methyl acrylate) (PMA) or poly(ethylene glycol) methacrylate (PEGMA) was chosen as the matrix material to replace the PAAm hydrogel, and similar responses were realized when the film was stretched.[143,144] The deformations as well as the diffraction of mechanical RPCs are usually reversible once the stress is released, while the recovery time depends on the elastic properties of the specific polymer matrix.

The wavelength tuning range of such mechanical RPCs is determined by the volume fraction of polymer content and stretching ratio (L/L_0). At a specific stretching ratio, a "soft" photonic hydrogel with higher polymer content exhibited a larger wavelength shift,[143] while for a PMA–silica film the diffraction gradually blue-shifted as the film was stretched to a ratio of 1.35. In order to increase the stretching ratio, Tsutsui and co-workers developed an inverse opal structure made of a pure PMMA hydrogel frame, which displayed an 80 nm peak shift as the film was stretched to a ratio of 1.6.[37] Fudouzi and Sawada have fabricated an elastic silicone sheet with reversibly tunable color by embedding a thin layer of PS colloidal crystals in poly(dimethylsiloxane) (PDMS).[145] As schematically shown in Figure 6a, when this sheet was stretched in the horizontal direction, it was reduced in size in the vertical direction, thus leading to the decrease in the lattice distance of (111) planes and consequently to the blue shift of the diffraction peak. Figure 6b shows that during stretching, the peak position shifted from 590 to 560 nm, and the reflectance intensity decreased gradually as indicated by the arrow. It has also been pointed out that when the stretching ratio is above a given value, the diffraction peak cannot be changed any further, as the colloidal particles come into contact with each other.

Although the mechanical RPCs discussed above showed reversible deformation and diffraction shifts, their mechanical performance was not satisfactory. Moreover, the recovery time of the deformation was relatively long (from several seconds to a few hours) owing to the elastic characteristics of

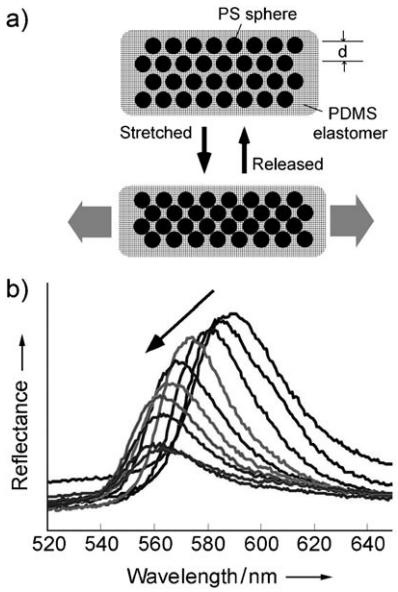

Figure 6. a) Reversible tuning by stretching of the lattice distance of a PS colloidal crystal embedded in a PDMS elastomer matrix. b) Relationship between the reflectance peak positions and elongation of the silicone rubber sheet by stretching. The peak position shifted from 590 to 560 nm, and the reflectance intensity decreased gradually as indicated by the arrow. From Ref. [145].

classic hydrogel that contains a high volume fraction of water. Recently, Foulger et al. developed a water-free, robust, and fast-responding composite by swelling the PEGMA–PS photonic hydrogel with 2-methoxyethyl acrylate (MOEA) with subsequent second-round photopolymerization.[146] As the final composite is composed mainly of polymerized MOEA (>80%), which roughly determines its transition temperature (T_g), and because MOEA monomer could be partially or completely substituted by other acrylates, the thermomechanical properties of this RPC could be tailored for stretching and pressing at different temperatures. Applying a 145 kPa compressive stress to the PMOEA-based film shifted the diffraction peak from 610 to 517 nm, and the stop band returned within 100 ms after the stress was released. When the PMOEA-based RPC was coupled to a piezoelectric actuator, the wavelength tuning range could be extended to a maximum of 172 nm for an applied 240 V bias, and the responding frequency could reach 200 Hz in an external field with square oscillations. Such mechanochromic response can also be coupled with the intrinsic electroactive properties of a dielectric thin film to realize a similar electrical response, especially when the permittivity of the PMOEA film is raised by incorporating Ag nanoparticles.[41]

4.4. Optically Responsive Photonic Crystals

Optical irradiation is a precise and effective stimulus to tune the structures of photonic crystals when photosensitive molecules are infiltrated into the system. Optical RPCs usually function through light-induced changes in lattice structure or the refractive index of the components. Sato et al.

reported a malachite green carbinol base (MG)-infiltrated silica colloidal crystal which exhibited photochemical control of the particle's arrangement by changing the free ion concentration and surface charge of the particles.[36] Upon UV irradiation (300 nm), the neutral MG molecules ionize into two charged fragments, MG^+ and OH^-, which screen the electrostatic forces between particles and cause an order-to-disorder phase transition (accompanied by the disappearance of diffraction) when the number of free ions exceeds a critical value. After irradiation, the ordered structure and the diffraction can be partially restored by a thermal process, but with decreased intensity and slightly increased interparticle distance.

Asher et al. fabricated optical RPCs with response in diffraction wavelength rather than intensity.[42,147] For instance, one of their optical RPCs is designed on the basis of the spirobenzopyran chromophore covalently attached to a polymer/crystal composite, whose photoisomerization upon UV or visible irradiation changes the hydrogel free energy of mixing owing to the alteration of charge distribution in the molecules, and thereby changes the volume of the composite in a dimethyl sulfoxide (DMSO) medium. The diffraction red-shifts as the spiropyran is excited with a YAG laser beam (355 nm), and blue-shifts as its UV isomer merocyanine is irradiated with an Ar^+ laser beam (515 nm). Little change occurs in the refractive index at these low spiropyran concentrations, and the diffraction shift is attributed to the volume change in the composite. The diffraction wavelength shift of approximately 13 nm between the two states is fully reversible, although it takes about 25 min to reach the equilibrium states.

Optical RPCs can also be realized by tuning the refractive index if the volume fraction of infiltrated spiropyran is high.[148,149] Sato et al. suggested that a large change in the stop band is achievable by illumination if a photochromic dye aggregate is chosen such that the electronic oscillation frequency of the aggregated state is close to the photonic band gap while that of the non-aggregated state is far from the gap.[148] They used the spiropyran derivative 1′,3′-dihydro-3′,3′-dimethyl-6-nitro-1′-octadecyl-8-docosanoyl-oxymethyl-spiro[2*H*-1-benzopyran-2,2′-[2*H*]indole] as the optically responsive dye. This dye molecule undergoes photoisomerization from the spiropyran form to the merocyanine form upon illumination with UV light and forms J-aggregates spontaneously in a thermal process. The J-aggregates of merocyanine formed after UV irradiation possess a wavelength-dependent refractive index that is higher at wavelengths above 600 nm and lower at shorter wavelengths than the constant refractive index of spiropyran. The change in refractive index causes a 37 nm red shift of diffraction for 275 nm silica opal (originally diffracts at 725 nm) and a 6 nm blue shift of diffraction for 195 nm silica opal (originally diffracts at 488 nm). The diffraction can be recovered by reversing the conformation change of the dye at 120 °C. The same group soon demonstrated the use of another spiropyran derivative, 1,3-dihydro-1,3,3-trimethylspiro[2*H*-indol-2,3′-[3*H*]naphth[2,1-b][1,4]oxazine] to realize similar wavelength tuning purely through light irradiation (UV and visible light).[149] Figure 7 shows the photoisomerization between

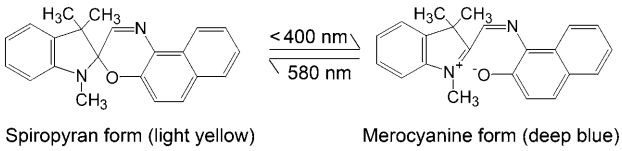

Figure 7. Photoisomerization of a photochromic dye between its spiropyran and merocyanine forms upon illumination of UV and visible light. From Ref. [149].

spiropyran and merocyanine forms upon illumination by UV and visible light. Although the reversible wavelength shift (ca. 10 nm) is smaller than that of the previous system, the switching can be rapidly achieved in 20–30 s. To improve the band shift in the future, the photochromic dyes might be designed to have large changes in refractive index around their electronic oscillation frequency.

In addition to photosensitive molecules, liquid crystals can also be introduced to generate responsive photonic crystals owing to their various responses to external alteration, including optical, thermal, and electric changes. Sato et al. have developed a diffraction on/off switchable optical RPC by taking advantage of the nematic–isotropic phase transition of a photochromic liquid crystal, 4-butyl-4′-methoxyazobenzene (AzoLC), which together with 4-pentyl-4′-cyanobiphenyl (5CB) was infiltrated into a silica inverse opal.[150,151] The reflection of this system is initially inhibited because of the bipolar structure in the nematic phase, which results in randomness of the dielectric constant and thereby light scattering. A *trans*-to-*cis* photoisomerization of AzoLC upon UV irradiation leads to the nematic-to-isotropic phase transition, which homogenizes the refractive index and allows the appearance of diffraction. Accordingly, the reflection can be turned off by reverse photoisomerization induced by visible light. The on/off switching can be performed with high reproducibility during the light irradiation cycles.

An interesting birefringent photonic crystal was fabricated when the same liquid crystals (5CB and AzoLC) were infiltrated into a stretched PMMA inverse opal.[152] In contrast to the bipolar structure, the LC molecules, when in nematic phase, align along the elongation direction. As a result, a great mismatch of refractive index along the stretching direction caused a reflection when a parallel polarized light illuminated the crystals, and the reflection gradually disappeared by rotating the polarization to the perpendicular direction owing to the decreasing contrast in refractive index. UV irradiation triggered a nematic-to-isotropic phase transition, which blue-shifted the diffraction peak for parallel polarized light and at the same time induced the appearance of diffraction for the perpendicular polarized light. Irradiation with visible light can reverse the phase transition from isotropic back to the nematic phase. Using two pieces of such films with different stop bands were stacked together with perpendicular elongation directions, Gu et al. demonstrated a photonic device that could be used to determine the polarization of incident light by the relative intensity of the two diffractions.

4.5. Electrically Responsive Photonic Crystals

4.5.1. Liquid-Crystal-Based Electrical RPC

Liquid crystals have a large optical anisotropy owing to their anisotropic molecular shapes and alignment. As such alignment is extremely sensitive to electric fields, photonic crystals infiltrated with liquid crystals have been widely investigated for the fabrication of electro-optical devices. Although many research efforts have been directed towards the applications of LC RPCs in advanced physics and optics,[153–158] we limit our discussion to the basic operation mechanisms.

As described above, the synthesis of LC-based electrical RPCs is usually carried out by infiltration of LC molecules into porous regions in photonic crystals. The tuning is typically achieved through the reorientation of LC molecules in an electric field. Shimoda et al. have reported a nematic LC (5CB) infiltrated silica opal structure whose diffraction peak can be blue-shifted by increasing the electric field. The shift in diffraction wavelength reached 5.5 nm upon the application of a 160 V electric field.[159] Such response originates from the molecular reorientation along the electric field, which aligns the LC molecules parallel to the direction of incident light, increases the ordinary part (n_o) of refractive index, and thereby decreases the average (effective) refractive index (n_{av}). Although theoretically the shift is expected to be larger if all the molecules can be completely oriented towards the electric field, in practice the reorientation is limited, as a large percent of LC molecules are immobilized near the surface of solid substrates. The electro-optic response of such LC RPCs to alternating electric fields is even faster than a conventional twisted nematic (TN) cell, as the rising time is on the order of microseconds and recovery time is in the millisecond range. In a similar silica opal structure infiltrated with liquid crystalline 4-(*trans*-4′-pentylcyclohexyl)-benzonitrile (PCH5), the Bragg diffraction exhibited an electric-field-induced blue shift when the molecular axis of the liquid crystal was parallel to the colloid surfaces, while no shift was observed for molecules normal to the colloid surface, which again confirmed the intrinsic relationship between molecular orientation and refractive index in the LC RPC.[32]

Compared with the opal structure, the inverse opal offers a larger empty volume (ca. 74%) for infiltration of liquid crystals. The enhanced optical anisotropy is therefore expected to yield a larger tunability under electric modulation. Ozaki et al. reported a 5CB infiltrated polymer inverse opal matrix which displayed a similar blue shift of reflection in response to an increasing electric field (Figure 8).[160] Upon the application of a voltage of 300 V, a large shift of 35 nm was induced, which was attributed to the large volume fraction of LC molecules in the voids. A threshold of applied voltage around 150 V can be observed, below which the reflection hardly shifts and above which it monotonously blue-shifts. With the enhanced tuning range, the response time is still comparable to that of a conventional twisted nematic cell (1–2 ms). When a low-refractive-index liquid crystal is infiltrated into an inverse opal framework made from a material with a high dielectric constant such as silicon, the orientation tunability of the LC plus the large dielectric contrast may cause the 3D photonic band gap to completely open or close upon application of an electric field.[161]

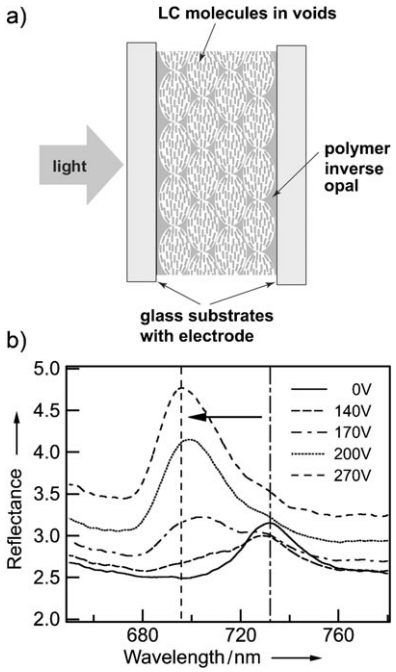

Figure 8. a) Schematic illustration of liquid-crystal-infiltrated polymer inverse opal film sandwiched by two transparent electrodes. b) The reflection spectra showing the dependence of diffraction upon the applied electric field. From Ref. [160].

4.5.2. Electrochemical Electrical RPC

Recently, Ozin et al. reported a unique electrical RPC that was constructed using an opal structure and a cross-linked metallopolymer network with a continuously variable degree of oxidation.[162] The design originates from their earlier report describing the composite film responding to chemical redox agents by redox-induced solvent swelling. Such response can be further improved and simplified by substituting positive or negative electrical potentials for the redox agents.[163] In a typical synthesis, silica colloidal crystals were first infiltrated with a mixture of di- or trifunctional thiol, photoiniator, and polyferrocenylsilane (PFS) derivatives with pendant C=C bonds, such as polyferrocenylmethylvinylsilane (PFMVS) and polyferrocenyldivinylsilane (PFDVS). When exposed to UV light, the mixture polymerized to form an infinite metallopolymer network through a thiol–ene cross-link reaction. The polymer/silica composite film was sandwiched between indium tin oxide (ITO) glass slides, filled with organic solvent-based electrolyte, and sealed with epoxy.[162] When an oxidative potential is applied to the composite film, electrons are extracted from the iron atoms in the PFS backbone. At the same time, anions from the electrolyte diffuse into the polymer to neutralize the produced positive charges. Accompanying solvent injection swells the polymer and red-shifts the diffraction of the photonic system. In contrast, a reducing potential injects the electrons back into the polymer and expels the anions as well

as the solvent out, thus blue-shifting the diffraction. The cycling stability of the film was shown to be good, with sustained photonic performance in a series of 100 oxidation–reduction cycles. The switching between two diffractions can be completed in seconds, and the electrical bistability of the film is supported by the fact that the diffraction peak position can maintain for approximately 2 h after the electric field is removed.

An intrinsic disadvantage of the silica/PFS film is the difficulty for the electrolyte to permeate through a silica opal lattice whose voids have already been filled with polymer gels. The relatively dense film impedes the transportation of electrons and ions, prolongs the responding time, decreases the tuning range, and increases the voltage that is needed to drive the device. An inverse opal structure composed of pure PFS metallopolymer network (Figure 9a) was designed to

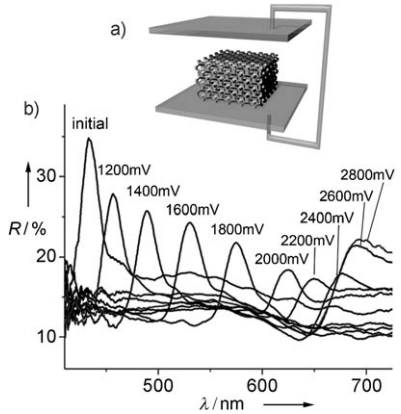

Figure 9. a) Scheme of the electrochemical cell fabricated for the electric actuation of RPCs. b) Relationship between the diffraction of an electric RPC and the applied voltage. From Ref. [164].

solve this problem.[164] The overall performance was greatly improved: the original silica/PFS composite film with 0.5 mol% cross-linker displayed a 210 nm shift in diffraction under an applied bias of 3.2 V, while a PFS inverse opal film with 5 mol% cross-linker exhibited a larger shift of 300 nm with a smaller bias of 2.8 V (Figure 9b). It should be noted that a higher degree of cross-linking in the polymeric RPC usually decreases the diffraction tuning range, so it is an exciting result to produce RPCs with a wide tuning range without sacrificing the system stability (by decreasing the cross-linking degree). The impressive performance is believed to result from the highly porous structure, which increases the specific area of the film in contact with electrolyte and promotes the transportation of electrons and ions. These important studies have stimulated the development of other electrochemical RPCs, such as the polypyrrole-based inverse opal.[165]

Besides the redox-active matrix, polyelectrolyte hydrogel can also be used to prepare electrical RPCs. As described previously, a porous poly(NIPAm-*co*-MAAc) film with an inverse opal structure exhibited electrochemically triggered rapid two-state switching between two arbitrary colors at a fixed temperature.[120] The photonic response is caused by a spatial–temporal change in pH value in the vicinity of the electrode around the film during the electrolysis process. A 1.8 V applied voltage decreases the pH value to 3.8 within 15 min at the anode, where the excessive H^+ ions inhibit the dissociation of methacrylic acid. The decreased Donnan osmotic pressure leads to the shrinkage of the hydrogel and a blue shift of the diffraction of 220 nm. Importantly, the shrinkage state can be maintained as long as electrolysis continues. However, this system also has limitations such as a large volume change with color change, poor durability, and a slow response.

Another type of polyelectrolyte electrical RPC is designed on the basis of the electrophoretic force-induced contraction of a hydrogel film.[166] A poly(HEMA-*co*-MAPTA-PF_6) hydrogel film prepared by the copolymerization of 2-hydroxyethyl methacrylate and [3-(methacryloylamino)propyl]trimethylammonium hexafluorophosphate is encapsulated between a carbon cathode and an ITO anode and then filled with a mixed solvent of dimethylformamide (DMF) and 1,4-dioxiane. Upon the application of an electric field, the electrophoretic force exerted on the cationic polymer backbone leads to the contraction of the inverse opal along the thickness direction and thereby reduces the lattice spacing. MAPTA-PF_6 was introduced to guarantee the dissociation of ions and charging of the polyelectrolyte matrix, considering the weak ionic interaction between $MAPTA^+$ and PF_6^-. A typical diffraction shift (12 V bias, in DMF) of 60 nm is acceptable for an optical switch configuration, but the relatively large driving voltage (10–30 V), slow response (ca. 60 s to reach equilibrium state), and the red shifts of diffraction during the cycling tests are potential concerns for practical applications.

4.6. Magnetically Responsive Photonic Crystals

4.6.1. Building Blocks and Particle Interactions

Magnetic RPCs are a special case when compared with all the other RPCs prepared by coupling ordered structures with the responsive materials. In such systems, magnetic components are usually directly incorporated into colloidal building blocks that can respond to external fields without any additional special treatment.[167–169] As the responsive mechanism is integrated into the building blocks, the performance of magnetic RPCs, such as the tuning range, response time, and so forth, is closely related to the properties of the specific magnetic colloids.[170] The following requirements have to be considered in constructing a magnetic RPC: 1) The colloids are expected to possess a uniform shape, a controllable size, and a narrow size distribution so that the lattice constant can be precisely tuned and crystal defects can be eliminated as much as possible. 2) Materials with high refractive-index contrast to the surrounding medium are needed to obtain strong diffraction intensity. 3) Superparamagnetism of the colloids is essential for achieving reversible optical response, because significant magnetic interactions need to be initiated only through the application of external magnetic fields. 4) Colloidal particles made of pure magnetic materials with a high saturated magnetic moment are preferred, as they will

favor a faster response to the external magnetic field and a lower responsive field strength threshold. 5) These magnetic particles are also expected to have appropriate surface properties that not only render the particles highly soluble in the dispersion medium but also produce sufficient repulsion to balance the magnetically induced attraction during the self-assembly process.

The ordered structures of magnetic RPCs can be formed with or without the presence of external magnetic fields. The magnetic tuning is usually achieved by changes in the interparticle spacing or the crystal structure through the magnetically induced particle interactions. Apparently, a non-close-packed colloidal assembly embedded in an easily deformable matrix such as a liquid is required to achieve dynamic structural tuning. Typically, the application of a magnetic field to a solution containing magnetic colloids induces a magnetic packing force $F_m = \nabla(\mu B)$ that drags the particles toward the maximum of the local magnetic gradient, a magnetic attractive force $F_{ma} = 6(\mu^2/d^4)$ between two adjacent particles lined up along the magnetic field, and a repulsive force $F_{mr} = 3(\mu^2/d^4)$ between two particles that are arranged perpendicular to the field, where μ is the induced magnetic moment, B is the strength of the external field, and d is the interparticle spacing.[171] The highly charged surface of colloidal particles usually generates an electrostatic repulsive interaction $F_{er} = \pi\varepsilon\zeta^2\kappa r e^{-\kappa h}$, where ε is the dielectric constant, ζ is the zeta potential, κ^{-1} is the Debye–Hückel length, r is the particle radius, and h is the interparticle surface-to-surface distance. If these forces are comparable in strength, any change to the force balance would alter the interparticle separation and assembly structure. There is no doubt that tuning by varying the strength of an external magnetic field can be conveniently carried out in a reversible manner. The advantages of magnetic fields as stimuli also include contactless control, instant action (in contrast to systems that involve slow diffusion of species such as solvents or ions), and easy integration into electronic devices.

4.6.2. *Magnetic Tuning of Preformed 3D Colloidal Crystals*

The early versions of magnetic RPCs were limited to magnetic tuning of preassembled colloidal crystals. Owing to the relatively low density of magnetic components in the colloidal building blocks, it has been difficult to order the particles directly using magnetic fields. Asher et al. have developed a magnetically controllable photonic crystal through the self-assembly of highly charged, monodisperse, and superparamagnetic PS colloids that contain 17 wt% iron oxide nanoparticles.[171,172] In the absence of a magnetic field, these particles self-assemble in deionized water into non-close-packed crystalline structures in a confined space by taking advantage of the strong electrostatic repulsive interactions. In this case, the lattice constant is determined by the particle number density and the crystal symmetry. When a magnetic field was applied, the preformed colloidal crystal showed magnetically responsive diffraction because of the disturbance of magnetic interaction in the originally established force balance, as schematically shown in Figure 10. A blue shift of diffraction from 560 to 428 nm was observed in an increasing magnetic field gradient from 1.5 to 5.4 kOe cm^{-1}. The peak shift corresponds to a decrease in (111) plane spacing of the colloidal crystal from 206 to 153 nm.

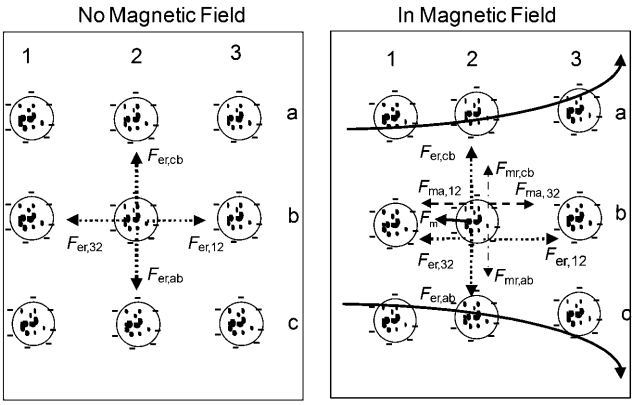

Figure 10. Forces on superparamagnetic particles within a colloidal crystal array in the absence and presence of a magnetic field. F_{er} electrostatic repulsive force, F_{ma} magnetic dipole–magnetic dipole repulsive force, F_m external magnetic force, F_{mr} magnetic dipole–magnetic dipole attractive force. From Ref. [171].

Although field-responsive photonic properties were realized, the volume fraction of the magnetically active materials was low so that the initial ordering of the particles could not be induced through the application of magnetic fields. The colloidal crystals preconstructed using the conventional self-assembly process, although non-close-packed, still possess a relatively small interparticle separation, so that the magnitude of change that external magnetic fields can induce is limited. A solid form of this magnetic RPC was also investigated by transferring the colloidal crystal to a PAAm or PHEMA hydrogel matrix through thermal polymerization. However, along with the solidification process, the lattice expansion and contraction were significantly hampered so that only 10 nm shift in diffraction could be induced by the magnetic fields.

4.6.3. *Magnetic Assembly and Tuning of Chainlike Photonic Structures*

In principle, the coexistence of magnetically induced attractive interactions and electrostatic repulsive interactions provides ideal conditions for self-assembly of colloidal particles into ordered structures.[173] The key is to increase the magnetically induced attractive force by either using stronger magnets or enhancing the magnetic moment of each particle. For building a magnetic RPC with a wide tuning range, instant response, and low driving field strength, it is critical to start with building blocks with high magnetic content. Bibette et al. have found that emulsion droplets containing concentrated iron oxide nanoparticles can instantly organize into ordered structures in the presence of a magnetic field.[174,175] However, since emulsions are not thermodynamically stable systems, the long-term stability of the oil droplets against dissociation or aggregation is a concern for practical applications.

We recently developed a one-pot high-temperature polyol process for the synthesis of polyelectrolyte-capped superparamagnetic "colloidal nanocrystal clusters" (CNCs) of magnetite (Fe_3O_4) with controllable uniform sizes in the range of approximately 30 to 200 nm.[176] Each Fe_3O_4 CNC has a unique cluster-like structure composed of many interconnected primary nanocrystals of approximately 10 nm diameter so that the CNC retains their superparamagnetic behavior at room temperature even though its overall size exceeds the critical size distinguishing ferromagnetic and superparamagnetic magnetite (30 nm). Thanks to a layer of covalently bonded polyelectrolyte surfactants, the Fe_3O_4 CNCs possess a highly charged surface and disperse well in aqueous solution. As the entire cluster is composed of magnetite, these CNCs also show a much higher saturated magnetization and therefore a stronger magnetic response to external fields than the individual magnetite nanodots or magnetite/polymer composites. Integrated with these useful features, these Fe_3O_4 CNCs and their derivatives can readily assemble in almost any kind of solvent into photonic structures that display brilliant colors from red to blue when the strength of the applied magnetic field is increased.[67,177,178] Figure 11 shows photographs of colloidal photonic crystals self-assembled in water in response to a varying external magnetic field as well as the reflection spectra displaying the dependence of the diffraction peak on the sample–magnet distance. Such optical response to the external magnetic field is instant and fully reversible, and may cover a wide spectrum range (greater than 300 nm). In addition, the required field strength for realizing the ordering of CNCs and color tuning is typically in the range of 50–500 Gauss.

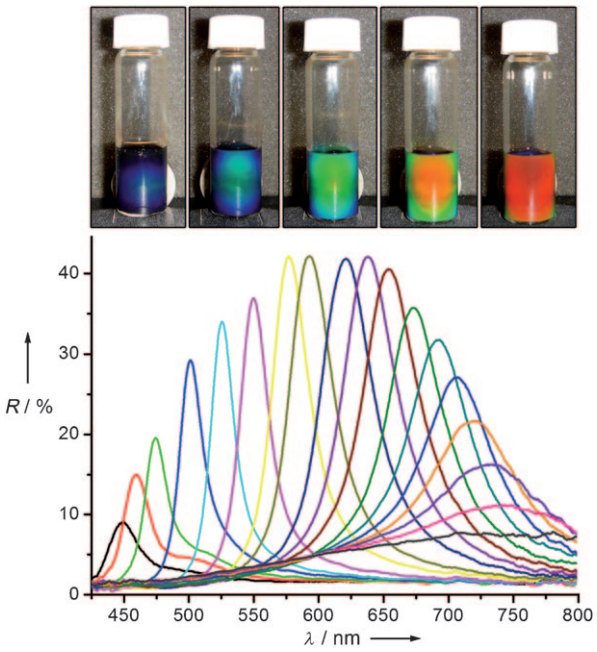

Figure 11. Top: Photographs of colloidal photonic crystals formed in response to an increasing external magnetic field (from right to left). Bottom: Dependence of the reflection spectrum on the sample-magnet distance. Diffraction peaks blue-shift as the distance decreases. From Ref. [67].

The magnetically assembled structures are parallel particle chains with periodic interparticle spacing, as determined by in situ optical microscopy of the assembly behavior (Figure 12 a,b).[68] The periodic arrangement of particles inside each chain has also been confirmed by fixing the assemblies in a polymer matrix and then inspecting a section that is cut from the composite along the chain direction (Figure 12 c).[179,180] This photonic structure, as schematically illustrated in Figure 12 d, is completely different from the 3D colloidal crystals discussed above. For example, in this case there is a much lower volume fraction of colloidal particles in solution (ca. 0.1 %).[68] The low particle density offers adequate room for instantly switching between the highly ordered and completely disordered states as well as for wide tuning of the interparticle spacing. The large contrast of refractive indices between magnetite and water is believed to be the major contributor for producing reasonably strong diffraction even in such diluted conditions.

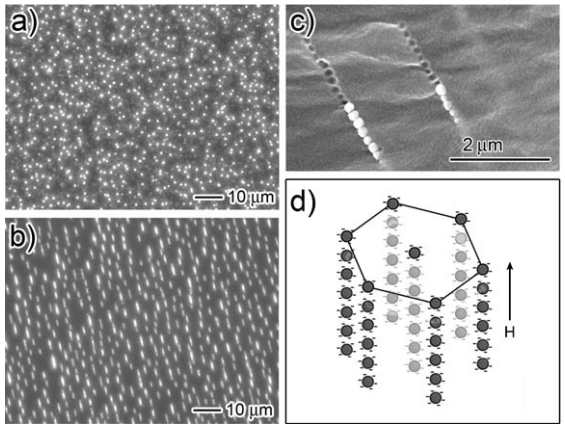

Figure 12. a,b) Dark-field optical microscopy images of Fe_3O_4 colloidal particles dispersed in a liquid film in an increasing external magnetic field. The superparamagnetic particles self-assemble into chains under external magnetic field. c) SEM images of silica-coated Fe_3O_4 particle chains fixed in a polymer matrix, which confirm the periodic arrangement of the particles inside each chain. d) Schematic illustration of the structure of Fe_3O_4 colloids self-assembled in the presence of an external magnetic field. From Ref. [68].

The key to the successful assembly of magnetic RPCs in aqueous solutions is the establishment of a balance between the field-induced magnetic attraction and the electrostatic repulsion.[67] In the direction perpendicular to the magnetic field, both electrostatic and magnetic interactions are repulsive, which keep the particle chains away from each other to prevent immediate aggregation until the magnetic packing force becomes dominant. In an increasing magnetic field, the enhanced magnetic attractive force causes the neighboring particles approach each other until the electrostatic repulsion becomes strong enough to balance the magnetic attraction, thus leading to a blue shift in the diffraction. In a decreasing magnetic field, the diffraction gradually red-shifts and eventually disappears when the colloids become disordered. The disorder–order transition and diffraction tuning are completely reversible.

For the assembly of magnetic particles in polar organic solvents such as ethanol, 2-propanol, and EG, a new mechanism of strong repulsive interaction is required, as the electrostatic interactions are greatly weakened and particles contact each other when the magnetic attraction is increased to a critical value.[177] In this case, the Fe_3O_4 CNCs were modified with a thin layer of SiO_2 to enable dispersibility in these solvents and generate a solvation layer around the particle through hydrogen bonding. A strong repulsive solvation force is established when two particles approach each other and their solvation layers overlap.[181,182] The electrostatic force remains effective at larger separations, and the solvation force dominates at small interparticle distances. As a result, the RPCs assembled in alcohols showed a skewed profile of the diffraction in response to the changes in the field strength, in contrast to the symmetric profile in an aqueous system.

The assembly of magnetic RPCs in nonpolar solvents has been a great challenge, since the electrostatic interaction in such a system is generally negligible. Achieving charge separation in nonpolar solvents is extremely difficult owing to the low dielectric constant and consequently higher Bjerrum length than that in water.[183,184] To create a strong electrostatic repulsion, we introduced charge control agents such as sodium bis(2-ethylhexyl)sulfosuccinate (AOT) to the nonpolar dispersions.[178] The resulting reverse micelles of a few nanometers in diameter can reduce the energy barrier of charge separation on the particle surface and also enhance surface charges by stabilizing their counterions in the micelles.[184–186] This long-range electrostatic repulsion can counterbalance the magnetic attraction and make it possible to assemble the Fe_3O_4@SiO_2 colloids modified with hydrophobic *n*-octadecyltrimethoxysilane (ODTMS) into tunable photonic structures. Compared with the aqueous and alcoholic solutions, the nonpolar system retains the fast and fully reversible optical response to the external fields, long-term stability, reasonably strong diffraction intensity, and wide tuning range (ca. 150 nm).

As the particle periodicity is determined by the force balance, any means that can cause changes in these forces may be used as stimuli to tune the photonic properties. A magnetic field is apparently the most convenient stimulus for this purpose because its strength can be controlled by the electrical current if electromagnets are used, or by controlling the sample–magnet distance if permanent magnets are used. Tuning electrostatic repulsion is also an effective method. For example, in a magnetic field with fixed strength, decreasing the ionic strength will increase the interparticle distance, therefore red-shifting the diffraction peak. But in practical settings, magnetic tuning is usually preferred because the strength of magnetic fields can be tuned within a broad range without interfering with the chemical environment. Most importantly, a strong interaction between the magnetic attraction and the electrostatic repulsion is always expected to acquire a high degree of order and thereby high diffraction intensity. The particle size also contributes to the control over the tuning range of the diffraction wavelength owing to the size-dependent magnetic moments.[68] Figure 13 compares the tuning range of photonic structures assembled from particles

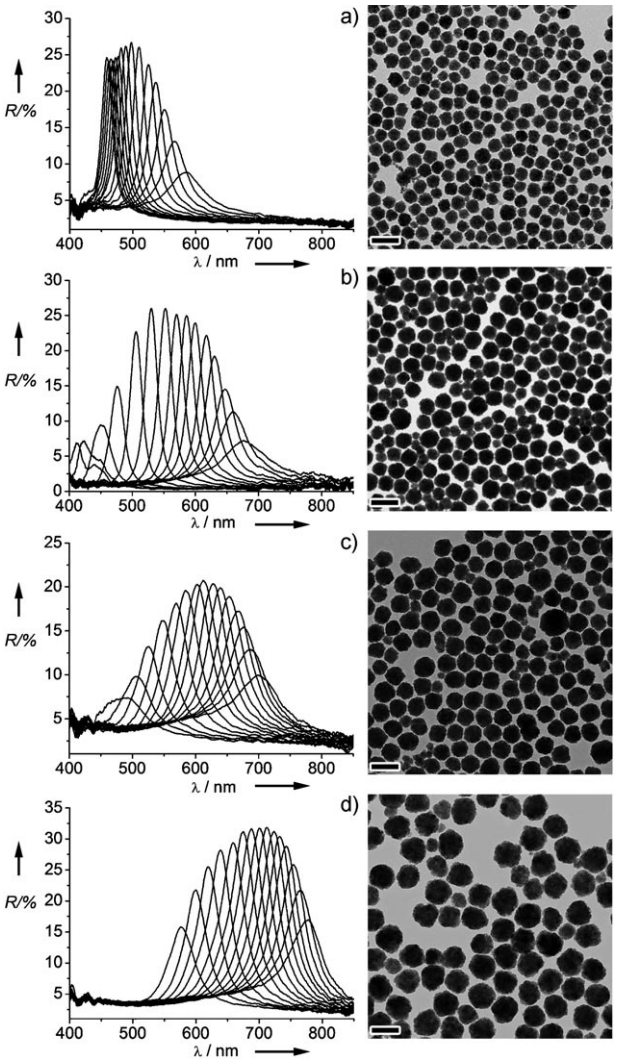

Figure 13. Diffraction of Fe_3O_4 CNC colloidal solution in response to magnetic fields with varying strengths. The tuning range of diffraction wavelength on particle size is compared for Fe_3O_4 CNCs with average diameters of a) 91, b) 108, c) 130, d) 180 nm. All scale bars are 200 nm. For each sample, the diffraction peak blue-shifts as the magnet–sample distance decreases. From Ref. [68].

with different average diameters. Generally, smaller CNCs (under 100 nm) form ordered structures only under strong magnetic fields and preferably diffract blue light. Larger clusters (over 150 nm) diffract red light in a relatively weak magnetic field, and the ordered structure may become unstable if the external field becomes too strong. Medium-size clusters (ca. 100–150 nm) self-assemble into stable ordered structures with tunable diffraction covering the entire visible spectrum.

The superparamagnetic colloidal dispersions display a fast optical response to external magnetic fields. When a solution of Fe_3O_4 CNCs is exposed to a periodically alternating magnetic field with a switching frequency of several hertz, the diffraction will switch on and off synchronically. Our recent measurement suggested a switching rate of approximately 30 Hz for the aqueous system. However, the diffraction intensity drops as the frequency of the external field increases,

because only short particle chains can form at higher frequencies, and it takes time for the short chains to merge into longer ones.

4.6.4. Magnetic Tuning of the Orientation of Photonic Crystals

The angle-dependent photonic-band-gap properties can also be employed to design tunable photonic systems. The general requirement is that the external stimuli should be able to induce an orientational change of the photonic crystals. The magnetic field seems to be a perfect choice for this purpose, as it can conveniently induce the rotation of solid objects containing magnetic components. Xia and Gates reported a thin slab of superparamagnetic photonic crystals fabricated through the assembly of polystyrene colloids in a commercial aqueous ferrofluid composed of magnetite nanoparticles (smaller than 15 nm) and subsequent calcination to remove the polymer template.[187] When suspended in an aqueous medium, the slab can be continuously rotated in or out of plane by controlling the orientation of a magnetic bar, and the diffraction blue-shifts as the sheet is tuned from horizontal to vertical orientation. Asher et al. also realized the orientational tuning of a magnetic photonic crystal film based on ferromagnetic materials.[188] A colloidal crystal made of ferromagnetic $CoFe_2O_4$/PS particles was embedded in an acrylamide hydrogel matrix through polymerization in the presence of a strong magnetic field. The magnetic moment of each particle was aligned along the external field, and their orientation was permanently locked to provide the film with a net macroscopic magnetic moment. The ferromagnetic composite film was then shredded into small fragments and dispersed into liquid medium. Application of a magnetic field along the detection probe caused the randomly oriented fragments to face up, thus significantly enhancing the diffraction intensity. Furthermore, two ferromagnetic composite crystal films with different lattice constants can be glued together and serve as a reversible photonic crystal mirror. A 180° rotation of the external magnetic field can switch the top and bottom face of the film, thus switching the reflection wavelengths.

For rapid and easy actuation, it is highly desirable that the magnetic photonic crystals can be divided into many smaller parts, the orientation of which can be controlled individually or collectively as needed. Recently, we developed so-called magnetochromatic microspheres composed of polymer matrix and ordered chains of superparamagnetic particles.[179] The microspheres were fabricated through instant assembly of superparamagnetic colloidal particles inside emulsion droplets of a UV-curable resin of poly(ethylene glycol diacrylate) (PEGDA) and immediate subsequent UV curing to polymerize the droplets and fix the ordered structures. As described, superparamagnetic Fe_3O_4@SiO_2 core–shell particles dispersed in the liquid droplets self-organize to form one-dimensional chains in magnetic fields. Each chain contains periodically arranged particles, diffracts visible light, and displays field-tunable colors. UV-initiated polymerization of the resin fixes the periodic structures inside the droplet microspheres and retains the diffraction properties. As shown in Figure 14, because the superparamagnetic chains tend to

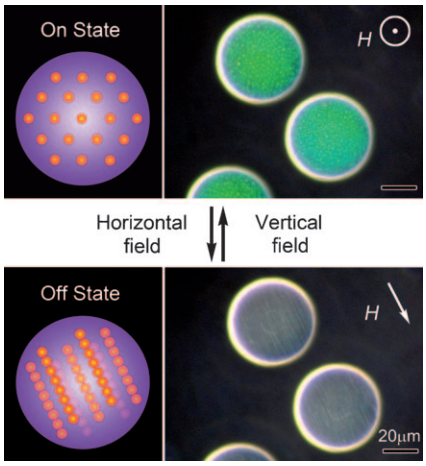

Figure 14. Schematic illustrations and optical microscopy images for the magnetochromatic effect caused by rotating microspheres containing chainlike photonic structures in magnetic fields. From Ref. [179].

align themselves along the field direction, it is very convenient to control the orientation of such photonic microspheres and, accordingly, their diffractive colors, by changing the orientation of the crystal lattice relative to the incident light using magnetic fields. Essentially, the diffraction of the microspheres can be conveniently switched between "on" and "off" states by rotating the spheres using an external magnetic field. By carefully controlling the direction of the external fields, the microspheres can also be kept at any intermediate stage between the on and off states with a specific tilting angle. The corresponding wavelength shift with the rotation angle matches well with Bragg's law. The excellent stability together with the capability of fast on/off switching of the diffraction by magnetic fields makes the system suitable for applications such as color displays, rewritable signage, and sensors.

4.7. Responsive Photonic Defects

Besides tuning the lattice constant, refractive index, crystal symmetry, and orientation, another strategy to produce RPCs the introduction of stimuli-responsive materials as defects, such as points, lines, and planes in 2D and 3D photonic crystals. Passive defects can be constructed by top-down methods, such as lithography,[54,189] two-photon direct writing,[190] holographic lithography,[13] and microrobotic manipulation.[191,192] Analogous to the stop-band tuning of defect-free photonic crystals, defect-mode transmission can also be controlled by most external stimuli that have been discussed above.

For example, liquid-crystal molecules can be sandwiched between two identical Bragg stacks as a defect layer. Then, the defect-mode transmission of such 1D photonic crystals can be controlled by manipulating the optical length of the defect layer through the reorientation of LC molecules in applied electric fields.[193] When a dye-doped nematic liquid crystal was deposited as a defect layer in SiO_2/TiO_2 Bragg stacks (Figure 15), a defect-mode laser emission excited by the irradiation of a pump laser beam (Nd:YAG) above the

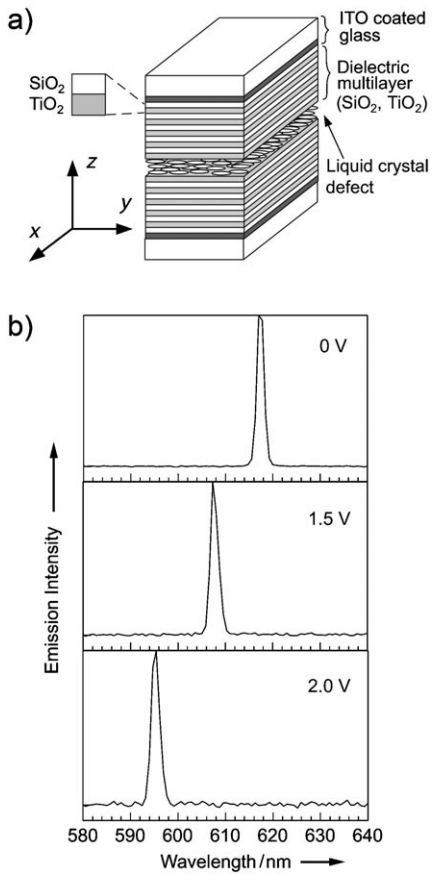

Figure 15. a) 1D photonic crystal composed of alternate multilayers of silica and titania with a liquid-crystal defect inside. b) Defect-mode transmission of 1D photonic crystals as a function of applied voltage. From Ref. [194].

energy threshold could be observed from the side opposite the incident light. The wavelength of diffraction blue-shifted upon application of an increasing electric field, again owing to the field-induced reorientation of the LC molecules.[194] A similar defect-state laser fabricated by replacing the dye-doped LC with conducting polymer as the emission layer also exhibited electrically responsive laser emissions. However, the intensity was not as high, as in this case the photons were strongly confined in the defect layer.[195]

3D colloidal crystals with poly(sodium styrenesulfonate)/poly(allylamine hydrochloride) (PSS/PAH) polyelectrolyte multilayers (PEMs) as a defect layer have also been reported to show responsive defect-mode transmission to chemical vapors.[196] One advantage of this method is that the well-established layer-by-layer technique allows precise control over the thickness of the PEM defect layers. By varying the partial pressure of water or acetone vapors, the defect-mode transmission can be reversibly tuned with nanometer precision, owing to the combined changes in the thickness of the PEM layer and the refractive index of the PEM layer. Similarly, the PEM defect layer constructed with a commercial polyelectrolyte of polydiallyldimethylammonium chloride and poly[1-[4-(3-carboxy-4-hydroxyphenyl)azobenzenesulfonamido]-1,2-ethanediyl, sodium salt] has shown responsive defect-state transmission under UV irradiation and temperature fluctuations because of the changes in the refractive index or lattice caused by photoisomerization and water desorption/absorption.[39] When the PEM defect layer is composed of PFS metallopolymer (Section 4.5.2), the defect transmission can even show a precise and reversible shift in the redox cycles.[197]

5. Application of Responsive Photonic Crystals

5.1. Photonic Crystal Sensors

The optical properties of RPCs can be tuned by various external stimuli through the manipulation of refractive index, lattice constant, crystal symmetry, and orientation. Their usefulness as sensors for detecting the presence of or change in stimuli is self-evident. Not surprisingly, a great number of studies have been reported for using RPCs as temperature, chemical, biomolecule, humidity, vapor, and pressure sensors. Interestingly, a good RPC does not always warrant a good sensor, because the objectives of making RPCs and sensors are not identical. For RPCs, the stimulus can be changed over a wide range to initiate a large photonic response, while for sensors, the photonic response needs to clearly identify the changes in the stimulus within a specified range. For example, a good chemical RPC may show a large diffraction shift when exposed to a high concentration of certain chemicals. However this RPC may not be a good sensor for detecting trace amounts of such chemicals in the environment. To use RPCs as sensors, it must be considered whether the sensitivity, response rate, durability, and selectivity of the responsive system can meet the specific requirements of the sensor application. Modifications or optimizations are usually needed to convert an RPC into a sensor. RPC-based sensors whose diffractions fall into the visible range are usually preferred, as the optical output can be directly observed by the naked eye without the need of complicated and expensive apparatus to read the signals.

5.1.1. Temperature Sensors

As discussed previously, hydrogel-based temperature sensors detect the temperature change by reading the diffraction shift of an RPC in response to thermally induced lattice expansion and shrinkage.[97,117,118] In contrast, inorganic temperature sensors utilize the photonic response arising from the phase-transition-induced change of refractive index to detect the temperature variation.[30,31,38,123]

Hydrogel-based sensors generally have better sensitivity, which means a larger diffraction-wavelength shift in response to the temperature changes, owing to the greater volume change of the polymer networks. These sensors have the intrinsic advantage in sensing the temperature in aqueous solution, making them suitable for many biological applications. In particular, hydrogels such as PNIPAM are biocompatible materials with a low toxicity, and their sensing range can be easily varied through chemical modification to match the temperature of the human body. Therefore, the mini-

aturized version of these smart, soft materials holds great potential as a temperature indicator for in vitro and in vivo experiments. Additional functions such as photothermal conversion and temperature-triggered drug release may be incorporated into these hydrogel sensors by including appropriate functional nanomaterials into the polymer network to create an integrated biomedical system that can diagnose, monitor, and treat diseases.

The inorganic sensors are good supplements to the hydrogel sensors, particularly when high-temperature detection and fast diffraction switching are required. Owing to the relatively high stability of inorganic materials, such sensors can indicate the temperature changes around their phase transition temperatures, which are usually above 100 °C. The switching of optical signals between two temperatures can be very fast, as the sensor is more durable at higher temperatures. The inorganic sensors can be made more responsive by using heating and cooling processes with large gradients, such as laser-induced microannealing, thus making them potential optical switches in optoelectronic devices. Such systems may also serve as thermal printable media, in which a phase transition can be induced in a confined region to produce patterns by laser irradiation and subsequent quenching to room temperature.[38]

5.1.2. *Ion and pH sensor*

Ion sensors are usually based on the bonding between the target ions and recognition groups attached to the hydrogel polymer network, which results in an increase of Donnan osmotic pressure and of the volume of hydrogel and in eventual red shift of diffraction wavelength. Typically, the ion sensor can be fabricated in the form of an optrode, which is made of an optical fiber with a small piece of ion RPC film attached to its end. Both the incident light from the light source and the backscattered light to the spectrometer propagate through the fiber perpendicular to the RPC film. The optrode usually works as a dip probe to monitor ion concentration.[44,124]

The sensitivity of an optimized ion sensor can produce an optical signal output with adequate resolution for spectrometer-level distinction. As demonstrated in a typical example of a Pb^{2+} sensor, the diffraction wavelength shifted about 160 nm as the concentration of Pb^{2+} ions increased from 20 ppb to 2000 ppm at moderate ionic strengths of a non-interfering electrolyte.[44] The RPC sensors are especially useful for the detection of trace amounts of ion species in the solution, as the shift in diffraction wavelength is approximately proportional to the logarithm of ion concentration. A slight change of concentration may cause apparent color changes. Besides metal-ion sensors, pH-value sensors can also be constructed by incorporating H^+-responsive polyelectrolyte, such as polyacrylic acid or polyacrylamide, into the hydrogel matrix.[111,119,127]

The response rate of ion sensors is usually determined by analyte diffusion and collective diffusion of the hydrogel network rather than by chemical bonding kinetics. For example, a Pb^{2+} RPC film with thickness of 125 μm can reach equilibrium within 30 s in a solution containing 1 mM Pb^{2+}, and the response time can be remarkably decreased to milliseconds by decreasing the film thickness to 10 μm.[44] Low cross-linking levels of the hydrogel network also contribute to enhanced response rate. Certainly, there is a limit for these manipulations in thickness and cross-linking level, because acceptably high diffraction intensity is still required for unambiguous detection.

The selectivity of ion sensors is largely determined by specific molecular recognition groups incorporated into the polymer network.[112,126] Currently, many ion sensors still suffer from the interference of one or two other ions, for example, Ba^{2+} ions were found to interfere with the selective detection of Pb^{2+} ions. In addition to the incorporation of more highly specific recognition groups, the selectivity may also be improved by combining several different types of sensors in the detection. By comparing the results from sensors with different recognition groups, it might be possible to identify the target ion.

As pointed out previously, high ionic strength is a major problem for the detection of ions with high concentration, because the increase in ionic strength decreases the Donna osmotic pressure in the matrix. Besides the swelling compensation strategy discussed above,[128,129] Asher and Reese have also optimized the construction of optrode probes to minimize the negative effect of high ionic strength.[125] As shown in Figure 16, the ion RPC film was polymerized onto a nylon mesh and sandwiched between the analyte solution and internal pure water of the optrode. After incubation of the optrode in analyte solution for some time, the tested side of the film was washed with water, thus relieving the blocks from the high ionic strength solution.

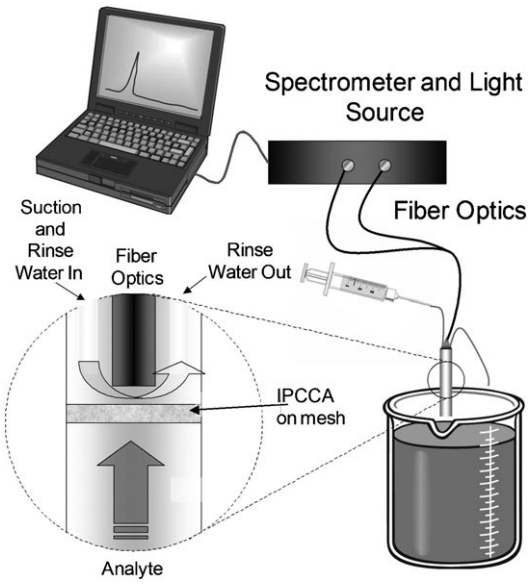

Figure 16. Optrode sensing device with cycling rinse water and responsive hydrogel / colloidal crystal composite film on nylon mesh substrate. After the optrode analyzed the concentration of chemical species in the outer solution, the inner rinse water is injected to regenerate the hydrogel film. From Ref. [125].

5.1.3. Solvent, Vapor, and Humidity Sensors

The quantitative analysis of solvents and vapors using RPC sensors is accomplished by the measurement of the diffraction wavelength shift caused by the change of effective refractive index associated with the infiltration of the analyte into the voids or pores in the photonic structure. Most of these sensors are fabricated in the form of inverse opals because of their larger pore volume for absorbing analytes, which leads to a larger change of refractive index and thereby better sensitivity. The porous structure also improves the diffusion of the analyte throughout the photonic structure, thus enhancing the sensor's response rate.[106,132,134–138]

The dependence of diffraction wavelength upon effective refractive index makes these sensors suitable for quantitative analysis. However, these sensors may not be able to provide enough information to identify two or more solvents with similar refractive indices when they coexist in a given system, because the shifts in diffraction wavelength are close to each other. In this case, 1D Bragg stacks composed of two kinds of alternating mesoporous layers may provide better resolution, because both the composition and surface properties of each layer can be manipulated to enhance the difference of responses to different solvents. For example, it was found that the difference in hydrophobicity of two layers, such as SiO_2 and TiO_2, helps to distinguish hexane and propanol even though they have the same refractive index.[134] Furthermore, the combination of photonic crystals with polymer matrices of different hydrophobicities can realize more interesting actuation in addition to sensing. Recently, et al. fabricated a reversible, color-tunable spiral photonic actuator by stacking two films together, one made of hydrophobic PDMS embedded in SiO_2 opal and the other a hydrophilic polyurethane/2-hydroxyethyl methacrylate copolymer.[198] The as-constructed thin polymer belt responded to both hydrophilic and hydrophobic environments not only by changing color but also by changing shape: it turned into left-handed spirals in hexane and right-handed ones in acetic acid.

RPCs in the form of inverse opals can be employed to sense not only solvents but also various chemical vapors. As the change in refractive index is determined by the filling ratio of the gaseous species, the vapor sensor actually measures the partial pressure of the vapor. A useful technical extension of such systems is the humidity sensor, which provides information of water vapor content in gaseous atmospheres.[35,142,199] Song et al. developed a humidity sensor by incorporating water-sensitive PAAm into a P(St-MMA-AA) photonic crystal template.[200] Photographs in Figure 17a demonstrate the reversible color change of the photonic crystal hydrogel in response to different humidities. It may serve as an economical alternative to traditional humidity sensors, as the film shows different colors covering the entire visible range in different humidity environments. As the sensor appears to be mechanically stable under cyclic humidity variations (Figure 17b), it can be made in the form of a flexible thin film and attached to many surfaces as an energy-saving humidity indicator.

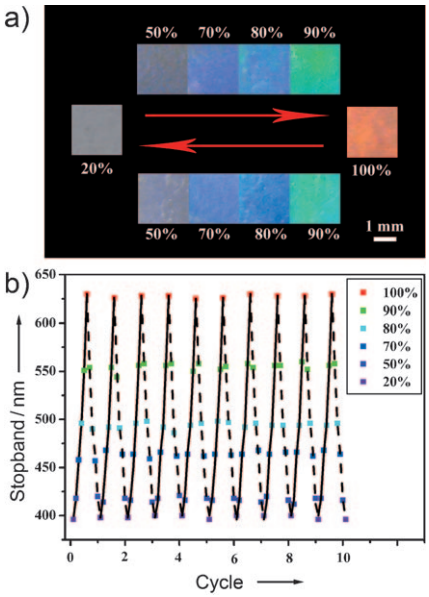

Figure 17. a) Photographs of PAAm-poly(St-MMA-AA) photonic hydrogel exposed to different humidities. b) Reversible conversion of stopband position of photonic hydrogel in ten successive cycles of increasing then decreasing the humidity. From Ref. [200].

5.1.4. Biological Sensors

Chemical RPCs can also be designed to identify biomolecules when appropriate recognition groups are attached. Figure 18 schematically illustrates the general mechanism of

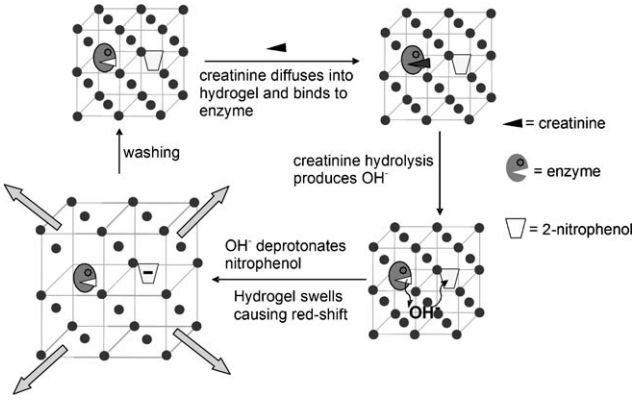

Figure 18. Schematic illustration of enzyme- and 2-nitrophenol-modified colloidal photonic crystal hydrogel as a biomolecule sensor responding to the creatinine in bodily fluids. From Ref. [128].

biological sensors using creatinine detection as an example.[128] A glucose sensor was the first prototype of a photonic crystal biological sensor. Asher and Holtz successfully demonstrated a glucose RPC by attaching the enzyme glucose oxidase (GO_x) to the polymer networks.[44] Thanks to the high selectivity of the enzyme, the glucose RPC has no response to analogous compounds such as sucrose or mannose. As the glucose solution swells the hydrogel film, the diffraction red-shifts owing to the increased osmotic pressure resulting from

the formation of a reduced flavin anion (GO_x^-) upon glucose turnover. In the absence of oxidants, the gel can detect glucose at concentrations as low as 10^{-12} M. However, in an oxygen atmosphere, reoxidation of flavin shrinks the gel and weakens the response of the RPC. Braun et al. fabricated a similar RPC by taking advantage of the charged complex formation between 1,2-*cis*-diol glucose and the phenylboronic acid groups attached to the hydrogel.[201] Interestingly, photonic crystals modified with boronic acid and poly(ethylene glycol) (or crown ether) respond to glucose molecules by blue-shifting the diffractions, since the supramolecular bis-bidentate glucose–boronic acid complex stabilized by PEG or crown ether-capped sodium cations can cross-link the polymer and shrink the hydrogel matrix.[202] The blue shift of the diffraction, an indicator of the degree of shrinkage, can be used to determine the concentration of glucose in the physiological environment.[202,203] Such cross-linking type sensors can respond to glucose at all physiological ionic strengths, while for sensors based on ion-induced expansion, the high physiological ionic strength can severely interfere with the determination of glucose concentration. The cross-linked glucose sensors have been further optimized and then incorporated into contact lenses to determine the glucose level in tear fluid. In this case, the body temperature accelerates the response kinetics and leads to fast detection within 5 min.[203] Based on diverse biological reactions, responsive photonic crystals have also been designed to detect many other biomolecules, such as sugars,[204] creatinine in bodily fluids, and organophosphorus compounds (Figure 18).[128,205]

Photonic crystal sensors are also capable of detecting not only simple biological compounds but also large biomolecules such as proteins and DNA.[206–210] For better flexibility, fast diffusion of the analyte, and higher sensitivity, these sensors can also be prepared in the form of suspension arrays, that is, encoded microspheres or beads dispersed in a solution, by colloidal crystallization in droplet templates.[206,207] Label-free silica inverse opal photonic beads (Figure 19) were prepared to detect tumor markers, such as Human CA125, CA19-9, and CEA.[208] The antibody probe immobilized on the pore surfaces of the photonic beads specifically binds the target antigen, thus resulting in a change of the refractive index of the beads and therefore a peak shift of corresponding diffractions. The detection may not require a decoding process and can be accomplished through direct measurement of the reflection of photonic beads in a flow-through microfluidic channel. A similar SiO_2/PEGDA opaline photonic bead labeled with oligonucleotide probes was developed to detect the oligonucleotide target based on the highly selective DNA hybridization.[209] These sensors may offer alternative medical diagnostic tools for early screening of various cancers, viruses, and genetic diseases.

Responsive photonic crystals can combine detection with other biological functions. For instance, metallodielectric Bragg stacks containing silver nanoparticles have been developed as both antimicrobial materials and label-free probes.[211] Owing to its low toxicity to human cells and convenient incorporation into various materials, silver has become a popular antibacterial agent that owes its activity to the interaction of silver ions with thiol-group-bearing proteins in bacterial cell membranes. When silver nanoparticles were introduced to TiO_2/clay BSs through $AgNO_3$ impregnation and a $NaBH_4$ reduction process, the stop band red-shifted 80–100 nm because of the increased refractive index and lattice spacing caused by Ag filling. When such a film was brought into contact with an agar medium inoculated with Escherichia coli, the film slowly released Ag ions and gradually blue-shifted its reflection to the original state, thus producing a zone of inhibition of roughly 3–4 mm. In this way, the TiO_2/clay 1D photonic crystals hybridized with Ag nanoparticles showed a tunable photonic stop band depending on the loading or releasing of Ag species. At the same time, the film can serve as an antimicrobial agent whose stocking is observable, which can be integrated into food containers or medical devices to prevent and indicate bacterial contamination.

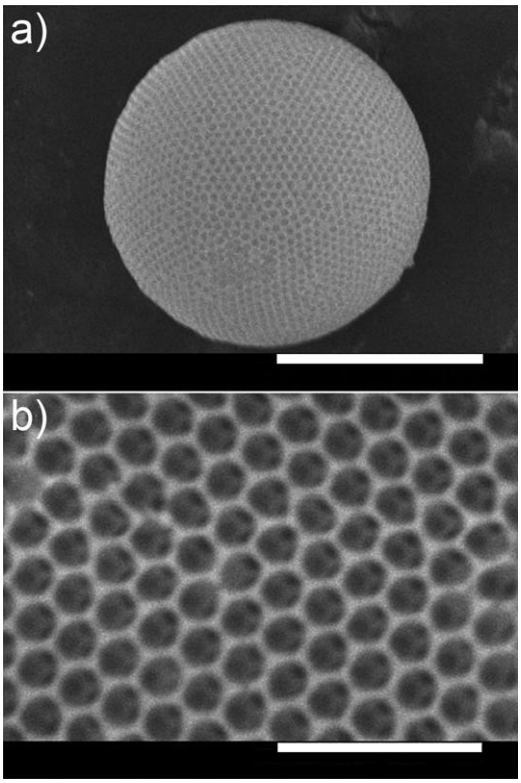

Figure 19. SEM images of a) inverse-opaline photonic beads composed of b) ordered interconnected pores inside the bead. From Ref. [208]. Scale bars: a) 5 μm, b) 1 μm.

5.1.5. *Pressure Sensors and Fingerprint Readers*

Photonic response to the mechanical deformation of elastomeric photonic crystal composite structures can be utilized to construct pressure sensors.[37,110,143,144,146] Most of these pressure RPCs are solid materials composed of colloidal crystals and soft polymeric frames so that a compression or stretching along one direction must be accompanied by an expansion or contraction along perpendicular directions to maintain a constant volume. Generally, a large compressive

stress is required to maintain the deformation (for example, a 145 kPa compression causes 100 nm shift for a PMOEA film), and the diffraction quickly recovers once the stress is removed.

Ozin et al. recently prepared a porous pressure-sensitive photonic crystal film by building elastomeric alkyl methacrylate or alkyl acrylate inverse opals using a templating strategy.[212] Owing to the porous characteristics, the dimension of the photonic crystals within the (111) planes does not change very much, while the (111) spacing decreases from 276 to 188 nm and the cross section of the voids changes from circular to ellipsoid under compression. As a result, the deformation of porous inverse opal films is relatively easy: a 15 kPa compression causes a blue shift of the diffraction peak by 60 nm. Since the redistribution of stress is greatly weakened in the porous film, feature sizes down to 5 μm can be distinguished when a patterned elastomeric stamp is pressed on the porous film.

Owing to the low compressive threshold and high resolution of distribution of compressive forces, such porous films might be further developed into a new generation of biometric recognition devices: fingerprint readers. After the finger was pressed on the film, videos were captured at 29 frames per second, providing 174 separate images for analysis over a 6 s press-and-release interval. The results showed not only the characteristic line ridges (Figure 20) but also the pressure distribution over the finger surface, which could be helpful to distinguish the imprint of a real finger from that of a rubber replica. Such fingerprint readers can be reversibly used for many cycles and provide accurate and multichannel (pressure- and time-dependent) information for identification purposes.

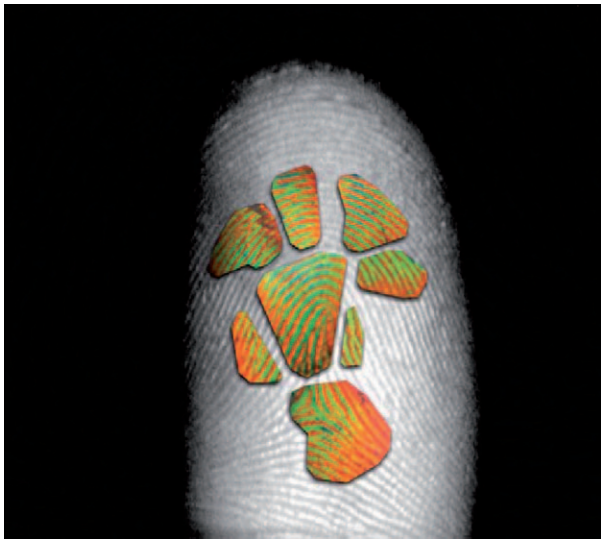

Figure 20. A full-color fingerprint visualized using an elastic photonic crystal, overlayed onto a grayscale image of an index finger. From Ref. [213].

5.2. Active Color Display Units

Photonic crystals with band gaps in the visible range can show brilliant colors and therefore hold great potential for many applications that require presentation of visual information. The structural colors produced by photonic crystals feature many unique characteristics that cannot be mimicked by traditional pigments, dyes, or phosphors, such as iridescence and metallic appearance. Also, they do not photobleach because they originate from the physical arrangement of the material. Furthermore, a single responsive photonic crystal may produce a wide range of colors. Such reflective-type displays work exceedingly well for outdoor usage such as signage and billboard advertising, where most emissive display technologies, such as liquid crystal, light emitting diode, and plasma displays have to struggle to overcome the problems such as high production cost, high energy consumption, and the annoying glare in sunshine. Although it is difficult to produce truly defect-free colloidal photonic crystal structures for optical telecoms, these photonic materials can adequately meet the requirements as color pixels in digital photographs, printing, and many display units. Since the human eye perceives color with a spatial resolution around 100 μm × 100 μm, the defects are usually tolerable at that dimension. The responsive photonic crystals introduced above bridge the optical signals and the external stimuli. While sensors are designed to use the optical signals to detect the changes in stimuli, display units tend to control the optical signals through the modulation of external stimuli.

5.2.1. Electrically Controlled Display Units

Their voltage-dependent photonic properties make electrical RPCs a natural choice for electrically controlled reflective display units. Recently, a prototypical full-color pixilated device was demonstrated using a composite material comprising an opal structure embedded in a matrix of redox-active polyferrocenylsilane gel.[162] When an oxidative or reductive potential is applied to the composite film, the polymer gel swells or shrinks accordingly, and thus an electric-field-driven display unit can be realized to reversibly show any color across the visible spectrum. Later, an inverse opal structure was prepared by removing the silica colloids in the SiO_2/PFS film to enhance the response rate, increase the tuning range, and decrease the voltage threshold for driving the device.[164] The capability of full-color tuning of such an electrical RPC in an electrochemical cell can be clearly seen in Figure 21. The impressive performance can be attributed to the highly porous structure, which promotes the transport of electrons and ions and increases the specific area of the film in contact with electrolyte.

The display unit in Figure 21 showed electrical bistable characteristics, which allow the diffraction to remain stable for approximately 2 h after removing the electric field, promising an energy saving display system. The power requirements to drive the display unit are impressively low with a voltage below 1.5 V and a current below 100 mA. It can also be fabricated on curved surfaces or integrated into flexible substrates to produce electronic paper. The technical

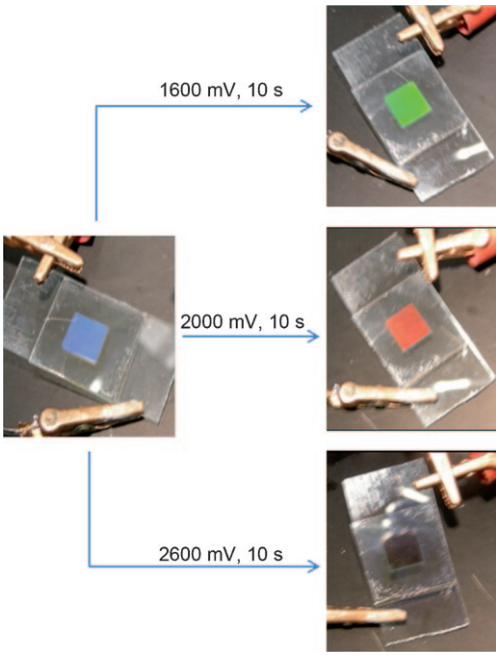

Figure 21. Full-color tuning of an electric RPC in an electrochemical cell. From Ref. [164].

challenges, which need to be addressed before the display units are released to the market, may include the durability, angle of visibility due to the angle-dependent diffraction, switching rate if used for video display, and the control of hue, lightness, and saturation of each pixel.[213]

5.2.2. *Magnetically Controlled Display Units*

An alternative method to realize a real-time display is magnetic modulation, as the strength and orientation of a magnetic field can also be easily controlled using electromagnets. This method also allows contactless control of the color pixels, which may be superior to electrical actuation in some respects. For example, a transparent electrode, typically made of expensive ITO glass, is usually required for electrically controlled photonic crystal displays. The use of ITO glass as electrodes also makes it difficult to fabricate flexible displays. Magnetically controlled display units, on the other hand, do not have these problems because the magnetic field can be applied remotely. The magnetically tunable photonic crystals that we have developed recently not only show different colors upon varying the strength of the magnetic field but also switch the diffraction between on and off states reversibly upon application and removal of the magnetic field. On the basis of this system we have further fabricated an elastic polymer film of magnetically responsive display unit by dispersing EG droplets containing Fe_3O_4@SiO_2 colloids in a solid PDMS matrix.[177] The superparamagnetic particles can self-assemble in the EG droplets when exposed to a magnetic field and change the diffraction color if the field strength varies. The film can also quickly switch its color between natural brown and a given color determined by the colloid size and the strength of the external magnetic field. The composite film retains the flexibility of the PDMS matrix and can be folded into various shapes while still displaying magnetically tunable colors. Thanks to the liquid nature of the PDMS precursors, the composite film can also be conveniently molded into different shapes and can exhibit predesigned patterns or letters with color contrast. Figure 22 shows the fabrication procedure for such a field-responsive photonic composite film as well as an example of a patterned film that can display letters in response to an external magnetic field. The limitations of this display system may include the relatively low response rate due to the use of viscous EG as the dispersion medium, the relatively weak reflectance due to the low number density of EG droplets in the PDMS matrix, and the long-term instability due to the slow evaporation of EG molecules through the polymer network.

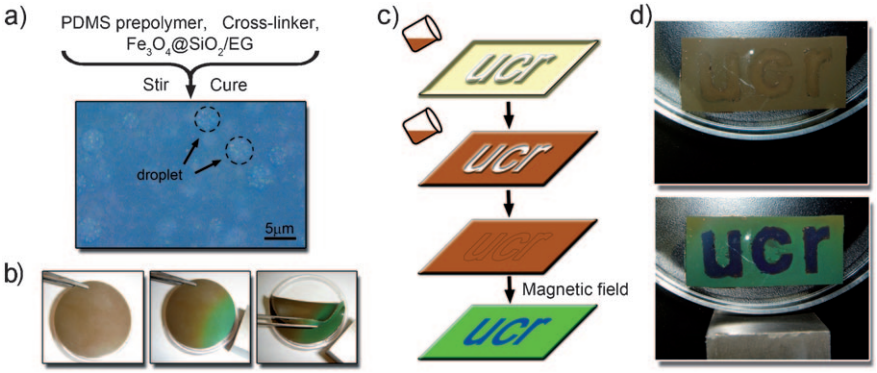

Figure 22. a) Fabrication procedure of a field-responsive PDMS composite embedded with droplets of EG solution of Fe_3O_4@SiO_2 colloids. The image shows an optical microscopy graph of the droplets under a vertically aligned external magnetic field. b) Magnetically induced color change of a flexible PDMS film. c) Schematic illustration of a two-step procedure for fabricating a patterned composite PDMS film that can display letters upon application of a magnetic field. d) Photographs of the as-prepared PDMS film prepared according to (c). From Ref. [177].

Magnetically controlled displays can also be realized by changing the orientation of photonic crystals through the external magnetic field. The magnetochromatic microsphere discussed in Section 4.6.4 is a good candidate for this purpose.[179] The embedded superparamagnetic particle chains make microspheres magnetically "polarized" and orientationally controllable, because the magnetic chains always tend to align along the direction of external fields. As a result, the diffraction of the microspheres can be conveniently switched between "on" and "off" states or restrained at any intermediate stage with a specific tilting angle by rotating the external magnetic field. Because the optical output of these microspheres can be collectively perceived, it is believed that

mixing of microspheres with RGB primary colors in different ratios may help to produce a broad array of colors. Compared with the dynamic nanoparticle assembly system, the magnetochromatic microspheres have several advantages, including the faster response with an adequately strong magnetic field (about 1000 G), long-term stability of the optical response, improved tolerance to environmental variances such as ionic strength and solvent hydrophobicity, and greater convenience for incorporation into many liquid or solid matrices.

5.3. Structural Color Printing

Photonic printing and inking are important technical extensions of responsive photonic crystals. For recording purposes, the structural colors of photonic crystal structures are more durable than traditional pigments and dyes. Unlike monitor-type display units, the printing and inking may not necessarily require instant color change, but it does require the photonic structure to be self-maintained in multiple color states for recording and energy-saving considerations.

5.3.1. Photonic Printing through Direct Assembly and Fixing

Among many strategies for photonic papers, ink-jet printing using a dispersion of monodisperse colloids and subsequent localized self-assembly of colloids on a substrate is probably the most straightforward method.[214–216] Although it integrates well with fully-developed ink-jet printing techniques, it has some limitations, such as the complex pretreatment of the paper surface, low flexibility of usable substrates, relatively high cost owing to its non-reusable nature, and the inevitable crystal defects and consequent inhomogeneous colors caused by environmental disturbance during the assembly process.

We recently demonstrated a fast and high-resolution color printing technique by combining magnetically tunable chain-like photonic structures with maskless lithography techniques.[180] A magnetic ink, called "M-ink", is a three-phase mixture composed of superparamagnetic Fe_3O_4@SiO_2 colloids, a solvation liquid, and a photocurable resin. Once an external field was applied, the magnetic colloids in the M-ink film assembled into chain-like structures, which were then fixed in the polymer matrix by the subsequent UV exposure without distorting the periodic arrangement of the colloids. The structural color was thus fixed. High-resolution patterning of multiple structural colors has also been explored by using a spatially modulated focused UV beam as the "printing" tool. Both the high-speed optical projection and magnetic field strength modulation were programmed so that the color of each exposed spot can be precisely controlled, eventually producing a high-resolution pattern of structural colors. Because of its instantaneous nature, photocuring allows localized solidification for high resolution patterning by avoiding significant free-radical diffusion during polymerization, making it possible to use techniques such as maskless lithography for creating arbitrary microscale patterns. With the help of a microelectromechanical system (MEMS)-based spatial light modulator, instantaneous illumination (in less than 80 ms) with patterned UV light can be applied for curing the resin.[217,218] Various multicolored patterns can be generated with a single ink by using a sequential process involving cooperative actions of magnetic field modulation and spatially controlled UV exposure. Micropatterns with different structural colors and geometries have been conveniently produced by repeating this "tuning and fixing" process, with examples shown in Figure 23. No movement of substrate was required since only one M-ink (instead of multiple color inks) was deposited at the beginning of the process. The scheme of generating structural color can be easily merged with well-developed reprographic techniques such as halftoning and dithering. Analogous to traditional grayscale expression, the overall reflection intensity can also be modulated by the number of color dots and present similar grayscale effects. Besides the intensity modulation, spatial color mixing has been shown to be possible by parallel distribution of dots with different structural colors. Quantized dot arrays composed of different colors can be seen as a single mixed color when their sizes are below the resolution of the human eye. It is therefore believed that this technique will provide a new platform for full-color structural color printing with fine resolution.

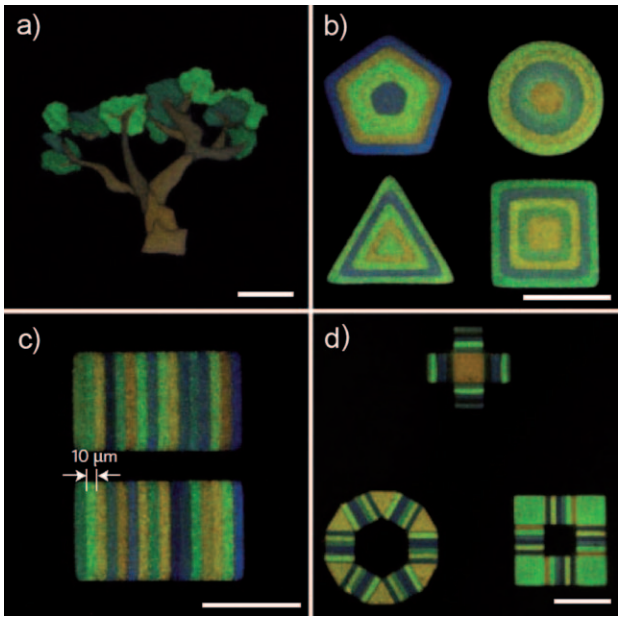

Figure 23. Printing of high-resolution patterns with multiple structural colors including a) a tree, b) concentric triangles, squares, pentagons, and circles, c) bar codes, and d) composite patterns of strip and polygon. Scale bars are 250 μm (a, d) and 100 μm (b,c). From Ref. [180].

5.3.2. Photonic Printing on Preformed Photonic Structures

A more general strategy for photonic printing is to define patterns on the preformed photonic crystal film. The printing processes can involve various methods that can change the stop band in a specific area with certain resolution to create a contrast of diffraction color in the form of letters and patterns.

For example, using photolithography techniques, pattern printing can be accomplished through the manipulation of the local refractive index, such as tuning of a liquid-crystal-infiltrated inverse opal film by UV-induced LC phase transition,[150,219] or by creating patterns on a silicon inverse opal film by laser-microannealing-driven phase transition of hydrogenated silicon.[123] The printing can also be realized by photoisomerization-induced polymer expansion and contraction.[121] When the porous P(NIPA-*co*-AAB) gel discussed in Section 4.1.1 was exposed to UV light through a photomask, the irradiated portion underwent a volume increase and accordingly a change in color (Figure 24a). As the swollen

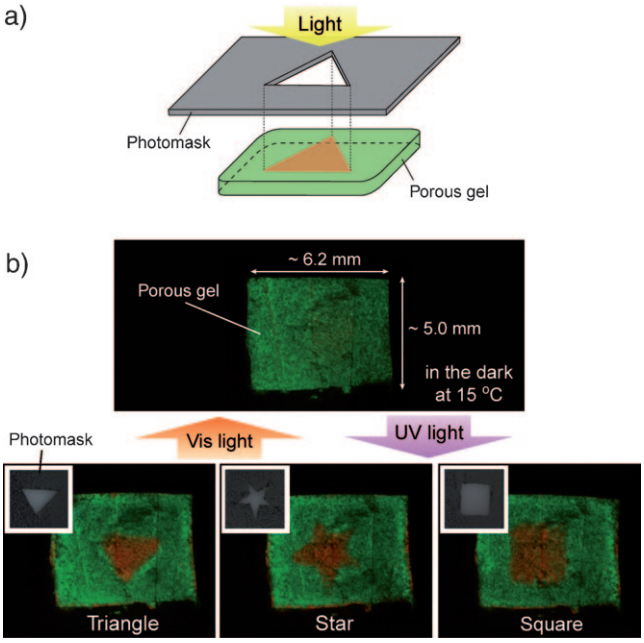

Figure 24. a) Schematic view and b) photographs of structural color printing on porous poly(NIPA-*co*-AAB) gel by iddradiation with UV light through a photomask. From Ref. [121].

portion has little influence on the volume of the nonirradiated portion, color patterns can be generated on the gel membrane (Figure 24b). These patterns can be erased and reproduced easily.

Thomas et al. suggested an interesting color printing strategy that utilizes the controllable distribution of cross-linking level in a hydrophobic block polyelectrolyte film and consequently different local swelling abilities to display color patterns in water.[220] In this case, polystyrene-*b*-quaternized poly(2-vinyl pyridine) (PS-*b*-QP2VP) 1D lamellar film was prepared through the self-assembly of block copolymer on substrate. Since the hydrophobic layer does not swell in water, the hydrophilic layer was forced to expand only along the normal direction, yielding extremely large diffraction wavelength tunability from 350 to 1600 nm through changes in both layer thickness and refraction index. To print letters or patterns, a second layer of 1D photonic crystal was deposited onto a preformed film by spraying the block copolymer solution with a different cross-linking level through the mask, which produced a pattern with a cross-linking level comparable to the original film. When the dry and transparent film was transferred to water, a flat color pattern appeared. Because each film layer was very thin, with typical thickness of several micrometers, different cross-linking levels led to different degrees of swelling and to different colors.

5.3.3. *Rewritable Photonic Paper by Solvent Swelling*

Writing on photonic paper can be simply realized by changing the lattice constant through solvent swelling. For instance, Xia and Fudouzi have developed a photonic paper/ink system using a PDMS/PS colloidal crystal composite film as paper and organic solvents as ink.[221,222] When the organic solvent was applied to the surface of the film, it swelled the PDMS matrix in selected areas, red-shifted the diffraction locally, and finally created a color contrast against the unswelled part. Such printing is easy to apply by either handwriting or contact printing with stamps. Figure 25

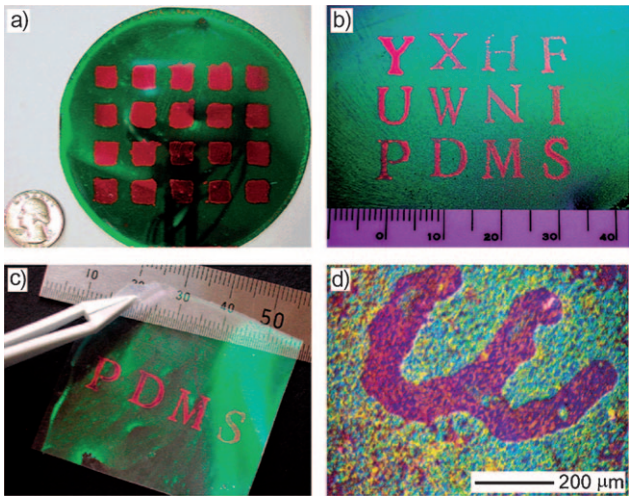

Figure 25. Patterns printed on the photonic papers with firm and soft substrates using silicone fluid as ink. The photonic paper was assembled from 202 nm PS beads in a PDMS matrix. From Ref. [221].

demonstrates that patterns with a striking contrast can be printed on the photonic papers with firm and soft substrates using silicone oil as ink. The limitation of such a system is that the color patterns may eventually disappear upon evaporation of the solvent even if a less volatile ink is used. Foulger et al. developed a similar PMOEA photonic paper using monomers as ink. The monomer ink swelled the PMOEA film and then created permanent ink marks after UV photopolymerization through a photomask.[223] This method effectively realized multicolor printing because monomers with different swelling abilities are readily available. It also dramatically enhanced the durability of ink marks. However, the toxicity of the monomers, which are usually highly volatile and cannot be completely converted into polymers by UV irradiation, might be a concern for practical applications.

A paper/ink system that follows the green chemistry principle can be realized by using water as an ink to write on

hydrophilic photonic crystal/polymer composite films. To make the ink mark stable, we have developed a rewritable photonic paper using a Fe_3O_4@SiO_2 particle chain embedded in PEGDA film as "paper" and an aqueous solution of hygroscopic salt such as LiCl, $MgCl_2$, $CaCl_2$, $ZnCl_2$, or $AlCl_3$ as an "ink".[224] Figure 26a schematically illustrates the

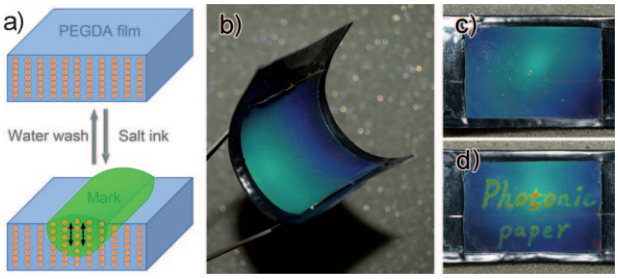

Figure 26. a) Schematic illustrations of the mechanism of writing or erasing realized by infiltrating or removing the hygroscopic salt. b–d) Digital photographs of flexible photonic paper (3×4 cm) on the plastic substrate with and without letters printed. The blank paper is uniform in color and the color gradient in the photos is caused by the flash lamp illuminating as a point light source. From Ref. [224].

mechanism of writing or erasing by using this method. Upon application, the ink swelled the polymer matrix, thus increasing the interparticle spacing within the chains and red-shifting the diffraction. As shown in Figure 26b–d, the color contrast led to a visible ink mark, which may last forever, as the solution can hardly evaporate at ambient temperature and humidity owing to the hygroscopic nature of the salts. As expected, the humidity has significant influence on the visibility of ink marks. Except in extremely low humidity environments, the ink marks were clear and visible. When required, the ink marks can be easily erased by rinsing the paper in distilled water to dissolve the residual salts. The interparticle spacing decreases after drying, thus blue-shifting the diffraction to its original state and making the photonic paper fully rewritable for many cycles. The entire writing and erasing process is safe for daily usage, as the photonic paper, salt ink, and rinsing water are nontoxic and environmentally benign.

The contrast in diffraction color is determined by the amount of hygroscopic salts introduced into the polymer matrix, thus providing a possible route for producing multi-color inks based on the degree of swelling. The current PEGDA polymer matrix has a relatively high degree of cross-linking so that the maximum swelling can yield a 100–150 nm shift in diffraction. Such a shift is enough to create a high color contrast but still not yet wide enough to cover the entire visible spectrum. With some chemical modification to the polymeric matrix, it should be possible to accomplish full-color writing using a single-component ink.

6. Summary and Outlook

We have summarized the recent developments in responsive photonic crystal structures, including the principles for design and fabrication and many strategies for applications. This is an exciting field with tremendous opportunities in both fundamental and technological aspects. Because many parameters described in the Bragg equation can be manipulated to change the photonic properties of a system, a number of fabrication methods are now available to realize responsive photonic structures with different characteristics. Even for tuning the same parameter, a large variety of completely different stimulating mechanisms can be employed to induce changes in photonic properties. Besides the direct applications of their visual effects, RPCs can also find uses such as optical switches, chemical and biological sensors, and anti-fraud devices.

As can be seen from many examples discussed in this Review, the majority of the RPC systems rely on self-assembly processes to achieve ordering. Compared with microfabrication techniques, self-assembly approaches have lower processing costs and higher production efficiencies. In particular, many self-assembly processes can be carried out in general research labs without the need for expensive instruments and strict processing conditions. This aspect also partially explains why in the past two decades there has been an explosion of new approaches demonstrated for the fabrication and applications of RPCs. However, the transition from laboratory to industrial practice requires large-scale manufacturing of these photonic structures in a highly efficient and reproducible manner. Major effort is still needed to further develop self-assembly approaches to meet the requirements for manufacturing. For example, the formation of high-quality colloidal crystals with large areas using current popular methods may still take hours to days or even months to complete. For many such processes, the sample size is intrinsically limited. Moreover, most of the assembly processes are not flexible in controlling the dimensions of the products. For example, the sedimentation and centrifugation processes do not allow precise control over the thickness of the samples, while the vertical deposition method is limited to the production of very thin films. Some advanced procedures may be able to produce photonic crystals with a relatively large area in a short period, but they usually involve special setups that make the remaining processing steps difficult. There is indeed a great need for developing simple and flexible processes that allow the rapid creation of photonic crystal structures on a large scale. In fact, some emerging techniques have already shown great promise in overcoming the above challenges. For example, the spin-coating method has shown the possibility of wafer-scale production of uniform colloidal photonic crystals.[80,81] The magnetic assembly approach developed in our group may also have the potential for mass fabrication on production lines. With some improvements, a flow-induced self-assembly process may eventually be able to create large-scale colloidal photonic crystals rapidly with high spectral quality.[225] The block-copolymer systems are also very promising for large-scale production, because their self-assembly is an intrinsically parallel process and can be flexibly applied on various substrates in large areas.

RPCs are of great commercial interest, as evidenced by the recent emergence of a number of start-up companies such

as Opalux, which is actively pushing the RPC-based photonic ink technology to the marketplace. Although many such niche applications have been successfully demonstrated, efforts are still needed to improve both the tuning range and response rate of the RPC systems for their even broader uses. For example, many hydrogel-based chemical RPCs showed a reasonably wide range of color change, but it takes tens of minutes or several hours to reach equilibrium, which is not acceptable for applications such as humidity sensors. When designing new systems with improved performance, it is always helpful to bear in mind the lessons learnt from natural photonic structures. For example, besides the intrinsic material properties such as elasticity and swelling capability, it is important to pay more attention to the surface properties and porosity of the designed RPC structures, which may significantly enhance the diffusion of stimulus species.

Some challenges in the application of RPC structures lie beyond the field of photonic crystals itself. For example, electrical RPCs have been regarded as very good candidates for color electronic papers because the color pixels can be individually addressed by electrodes patterned on substrates. However, the requirement for conductive and transparent substrates leads to very limited choices of materials such as the commonly used ITO, which is expensive and inflexible. The recent progress by using carbon nanotubes, oxide nanowires, graphene, or organic semiconductors for the fabrication of transparent thin-film transistors on flexible substrates represents an important step toward the required materials and circuitry for fabricating color electronic papers.[226–228]

Y.Y. thanks the University of California, Riverside and the US National Science Foundation for financial support. The donors of the Petroleum Research Fund, administered by the American Chemical Society, is also acknowledged for support of this research. Y.Y. is a Cottrell Scholar of the Research Corporation for Science Advancement.

Received: December 16, 2009
Published online: January 20, 2011

[1] S. John, *Phys. Rev. Lett.* **1987**, *58*, 2486.
[2] E. Yablonovitch, *Phys. Rev. Lett.* **1987**, *58*, 2059.
[3] E. Yablonovitch, *Sci. Am.* **2001**, *285*, 46.
[4] T. F. Krauss, *Nat. Mater.* **2003**, *2*, 777.
[5] Y. Akahane, T. Asano, B.-S. Song, S. Noda, *Nature* **2003**, *425*, 944.
[6] D. J. Norris, *Nat. Mater.* **2007**, *6*, 177.
[7] S. Y. Lin, J. G. Fleming, D. L. Hetherington, B. K. Smith, R. Biswas, K. M. Ho, M. M. Sigalas, W. Zubrzycki, S. R. Kurtz, J. Bur, *Nature* **1998**, *394*, 251.
[8] J. G. Fleming, S.-Y. Lin, *Opt. Lett.* **1999**, *24*, 49.
[9] S. Noda, K. Tomoda, N. Yamamoto, A. Chutinan, *Science* **2000**, *289*, 604.
[10] A. Birner, R. B. Wehrspohn, U. M. Gösele, K. Busch, *Adv. Mater.* **2001**, *13*, 377.
[11] H. Masuda, M. Ohya, H. Asoh, M. Nakao, M. Nohtomi, T. Tamamura, *Jpn. J. Appl. Phys.* **1999**, *38*, L1403.
[12] M. C. Wanke, O. Lehmann, K. Müller, Q. Z. Wen, M. Stuke, *Science* **1997**, *275*, 1284.
[13] M. Campbell, D. N. Sharp, M. T. Harrison, R. G. Denning, A. J. Turberfield, *Nature* **2000**, *404*, 53.
[14] S. Shoji, S. Kawata, *Appl. Phys. Lett.* **2000**, *76*, 2668.
[15] Y. Xia, B. Gates, Y. Yin, Y. Lu, *Adv. Mater.* **2000**, *12*, 693.
[16] R. C. Schroden, M. Al-Daous, C. F. Blanford, A. Stein, *Chem. Mater.* **2002**, *14*, 3305.
[17] C. López, *J. Opt. A* **2006**, *8*, R1.
[18] L. I. Halaoui, N. M. Abrams, T. E. Mallouk, *J. Phys. Chem. B* **2005**, *109*, 6334.
[19] A. K. Arora, B. V. R. Tata, *Ordering and Phase Transitions in Colloidal Systems*, VCH, Weinheim, **1996**.
[20] A. K. Arora, B. V. R. Tata, A. K. Sood, R. Kesavamoorthy, *Phys. Rev. Lett.* **1988**, *60*, 2438.
[21] P. Pieranski, *Contemp. Phys.* **1983**, *24*, 25.
[22] W. Van Negen, I. Shook, *Adv. Colloid Interface Sci.* **1984**, *21*, 119.
[23] Y. Yin, Y. Lu, Y. Xia, *J. Mater. Chem.* **2001**, *11*, 987.
[24] S. I. Matsushita, Y. Yagi, T. Miwa, D. A. Tryk, T. Koda, A. Fujishima, *Langmuir* **2000**, *16*, 636.
[25] Y. Fink, A. M. Urbas, M. G. Bawendi, J. D. Joannopoulos, E. L. Thomas, *J. Lightwave Technol.* **1999**, *17*, 1963.
[26] A. Urbas, Y. Fink, E. L. Thomas, *Macromolecules* **1999**, *32*, 4748.
[27] B. Comiskey, J. D. Albert, H. Yoshizawa, J. Jacobson, *Nature* **1998**, *394*, 253.
[28] Y. Chen, J. Au, P. Kazlas, A. Ritenour, H. Gates, M. McCreary, *Nature* **2003**, *423*, 136.
[29] S.-L. Kuai, G. Bader, P. V. Ashrit, *Appl. Phys. Lett.* **2005**, *86*, 221110.
[30] A. B. Pevtsov, D. A. Kurdyukov, V. G. Golubev, A. V. Akimov, A. A. Meluchev, A. V. Sel'kin, A. A. Kaplyanskii, D. R. Yakovlev, M. Bayer, *Phys. Rev. B* **2007**, *75*, 153101/1.
[31] J. Zhou, C. Q. Sun, K. Pita, Y. L. Lam, Y. Zhou, S. L. Ng, C. H. Kam, L. T. Li, Z. L. Gui, *Appl. Phys. Lett.* **2001**, *78*, 661.
[32] D. Kang, J. E. Maclennan, N. A. Clark, A. A. Zakhidov, R. H. Baughman, *Phys. Rev. Lett.* **2001**, *86*, 4052.
[33] S. W. Leonard, J. P. Mondia, H. M. van Driel, O. Toader, S. John, K. Busch, A. Birner, U. Gösele, V. Lehmann, *Phys. Rev. B* **2000**, *61*, R2389.
[34] P. Mach, P. Wiltzius, M. Megens, D. A. Weitz, K.-h. Lin, T. C. Lubensky, A. G. Yodh, *Europhys. Lett.* **2002**, *58*, 679.
[35] R. A. Barry, P. Wiltzius, *Langmuir* **2006**, *22*, 1369.
[36] Z. Z. Gu, A. Fujishima, O. Sato, *J. Am. Chem. Soc.* **2000**, *122*, 12387.
[37] K. Sumioka, H. Kayashima, T. Tsutsui, *Adv. Mater.* **2002**, *14*, 1284.
[38] U. Jeong, Y. Xia, *Angew. Chem.* **2005**, *117*, 3159; *Angew. Chem. Int. Ed.* **2005**, *44*, 3099.
[39] F. Fleischhaker, A. C. Arsenault, V. Kitaev, F. C. Peiris, G. von Freymann, I. Manners, R. Zentel, G. A. Ozin, *J. Am. Chem. Soc.* **2005**, *127*, 9318.
[40] S. O. Lumsdon, E. W. Kaler, J. P. Williams, O. D. Velev, *Appl. Phys. Lett.* **2003**, *82*, 949.
[41] J. Xia, Y. Ying, S. H. Foulger, *Adv. Mater.* **2005**, *17*, 2463.
[42] M. Kamenjicki Maurer, I. K. Lednev, S. A. Asher, *Adv. Funct. Mater.* **2005**, *15*, 1401.
[43] D. R. E. Snoswell, C. L. Bower, P. Ivanov, M. J. Cryan, J. G. Rarity, B. Vincent, *New J. Phys.* **2006**, *11*, 267.
[44] J. H. Holtz, S. A. Asher, *Nature* **1997**, *389*, 829.
[45] R. A. Potyrailo, H. Ghiradella, A. Vertiatchikh, K. Dovidenko, J. R. Cournoyer, E. Olson, *Nat. Photonics* **2007**, *1*, 123.
[46] J. Zi, X. D. Yu, Y. Z. Li, X. H. Hu, C. Xu, X. J. Wang, X. H. Liu, R. T. Fu, *Proc. Natl. Acad. Sci. USA* **2003**, *100*, 12576.
[47] S. Kinoshita, S. Yoshioka, K. Kawagoe, *Proc. R. Soc. London Ser. B* **2002**, *269*, 1417.
[48] P. Vukusic, J. R. Sambles, C. R. Lawrence, *Nature* **2000**, *404*, 457.
[49] M. Srinivasarao, *Chem. Rev.* **1999**, *99*, 1935.
[50] T. F. Krauss, R. M. de la Rue, S. Brand, *Nature* **1996**, *383*, 699.

[51] O. Painter, R. K. Lee, A. Scherer, A. Yariv, J. D. O'Brien, P. D. Dapkus, I. Kim, *Science* **1999**, *284*, 1819.
[52] H. Benisty, C. Weisbuch, D. Labilloy, M. Rattier, C. J. M. Smith, T. F. Krauss, R. M. de La Rue, R. Houdre, U. Oesterle, C. Jouanin, D. Cassagne, *J. Lightwave Technol.* **1999**, *17*, 2063.
[53] S. Noda, A. Chutinan, M. Imada, *Nature* **2000**, *407*, 608.
[54] S. Ogawa, M. Imada, S. Yoshimoto, M. Okano, S. Noda, *Science* **2004**, *305*, 227.
[55] D. N. Sharp, M. Campbell, E. R. Dedman, M. T. Harrison, R. G. Denning, A. J. Turberfield, *Opt. Quantum Electron.* **2002**, *34*, 3.
[56] O. Toader, S. John, *Science* **2001**, *292*, 1133.
[57] F. S. Bates, *Science* **1991**, *251*, 898.
[58] M. F. Schulz, A. K. Khandpur, F. S. Bates, K. Almdal, K. Mortensen, D. A. Hajduk, S. M. Gruner, *Macromolecules* **1996**, *29*, 2857.
[59] F. Marlow, Muldarisnur, P. Sharifi, R. Brinkmann, C. Mendive, *Angew. Chem.* **2009**, *121*, 6328; *Angew. Chem. Int. Ed.* **2009**, *48*, 6212.
[60] R. K. Iler, *The Chemistry of Silica*, Wiley, New York, **1979**.
[61] W. Stöber, A. Fink, E. Bohn, *J. Colloid Interface Sci.* **1968**, *26*, 62.
[62] E. Matijevic, *Langmuir* **1994**, *10*, 8.
[63] M. Ohmori, E. Matijevic, *J. Colloid Interface Sci.* **1992**, *150*, 594.
[64] W. P. Hsu, R. Yu, E. Matijevic, *J. Colloid Interface Sci.* **1993**, *156*, 56.
[65] A. P. Philipse, M. P. B. van Bruggen, C. Pathmamanoharan, *Langmuir* **1994**, *10*, 92.
[66] Y. Yin, Y. Lu, B. Gates, Y. Xia, *J. Am. Chem. Soc.* **2001**, *123*, 8718.
[67] J. Ge, Y. Hu, Y. Yin, *Angew. Chem.* **2007**, *119*, 7572; *Angew. Chem. Int. Ed.* **2007**, *46*, 7428.
[68] J. Ge, Y. Hu, T. Zhang, T. Huynh, Y. Yin, *Langmuir* **2008**, *24*, 3671.
[69] C. A. Murray, D. H. Van Winkle, *Phys. Rev. Lett.* **1987**, *58*, 1200.
[70] W. R. Bowen, A. O. Sharif, *Nature* **1998**, *393*, 663.
[71] P. A. Kralchevsky, N. D. Denkov, *Curr. Opin. Colloid Interface Sci.* **2001**, *6*, 383.
[72] K. D. Danov, B. Pouligny, P. A. Kralchevsky, *Langmuir* **2001**, *17*, 6599.
[73] A. J. Hurd, D. W. Schaefer, *Phys. Rev. Lett.* **1985**, *54*, 1043.
[74] F. Burmeister, C. Schafle, T. Matthes, M. Bohmisch, J. Boneberg, P. Leiderer, *Langmuir* **1997**, *13*, 2983.
[75] H. H. Wickman, J. N. Korley, *Nature* **1998**, *393*, 445.
[76] V. N. Paunov, P. A. Kralchevsky, N. D. Denkov, K. Nagayama, *J. Colloid Interface Sci.* **1993**, *157*, 100.
[77] T. Miwa, K. Nagayama, *Langmuir* **1999**, *15*, 5257.
[78] P. A. Kralchevsky, K. Nagayama, *Langmuir* **1994**, *10*, 23.
[79] H. W. Deckman, J. H. Dunsmuir, S. Garoff, J. A. McHenry, D. G. Peiffer, *J. Vac. Sci. Technol. B* **1988**, *6*, 333.
[80] P. Jiang, T. Prasad, M. J. McFarland, V. L. Colvin, *Appl. Phys. Lett.* **2006**, *89*, 011908.
[81] S. Venkatesh, P. Jiang, B. Jiang, *Langmuir* **2007**, *23*, 8231.
[82] M. Trau, D. A. Saville, I. A. Aksay, *Science* **1996**, *272*, 706.
[83] S.-R. Yeh, M. Seul, B. I. Shraiman, *Nature* **1997**, *386*, 57.
[84] Y. Solomentsev, M. Bohmer, J. L. Anderson, *Langmuir* **1997**, *13*, 6058.
[85] P. Jiang, J. F. Bertone, K. S. Hwang, V. L. Colvin, *Chem. Mater.* **1999**, *11*, 2132.
[86] M. Holgado, F. Garcia-Santamaria, A. Blanco, M. Ibisate, A. Cintas, H. Miguez, C. J. Serna, C. Molpeceres, J. Requena, A. Mifsud, F. Meseguer, C. Lopez, *Langmuir* **1999**, *15*, 4701.
[87] J. V. Sanders, *Nature* **1964**, *204*, 1151.
[88] K. E. Davis, W. B. Russel, W. J. Glantschnig, *Science* **1989**, *245*, 507.
[89] P. N. Pusey, W. van Megen, *Nature* **1986**, *320*, 340.
[90] H. Míguez, F. Meseguer, C. López, A. Mifsud, J. S. Moya, L. Vázquez, *Langmuir* **1997**, *13*, 6009.
[91] L. V. Woodcock, *Nature* **1997**, *388*, 236.
[92] S. A. Asher, P. L. Flaugh, G. Washinger, *Spectroscopy* **1986**, *1*, 26.
[93] P. L. Flaugh, S. E. O'Donnell, S. A. Asher, *Appl. Spectrosc.* **1984**, *38*, 847.
[94] R. J. Carlson, S. A. Asher, *Appl. Spectrosc.* **1984**, *38*, 297.
[95] T. Okubo, *Langmuir* **1994**, *10*, 3529.
[96] E. A. Kamenetzky, L. G. Magliocco, H. P. Panzer, *Science* **1994**, *263*, 207.
[97] J. M. Weissman, H. B. Sunkara, A. S. Tse, S. A. Asher, *Science* **1996**, *274*, 959.
[98] D. H. Van Winkle, C. A. Murray, *Phys. Rev. A* **1986**, *34*, 562.
[99] P. Pieranski, L. Strzelecki, B. Pansu, *Phys. Rev. Lett.* **1983**, *50*, 900.
[100] S. Neser, C. Bechinger, P. Leiderer, T. Palberg, *Phys. Rev. Lett.* **1997**, *79*, 2348.
[101] S. H. Park, D. Qin, Y. Xia, *Adv. Mater.* **1998**, *10*, 1028.
[102] S. H. Park, Y. Xia, *Langmuir* **1999**, *15*, 266.
[103] B. Gates, D. Qin, Y. Xia, *Adv. Mater.* **1999**, *11*, 466.
[104] J. D. Joannopoulos, S. G. Johnson, J. N. Winn, R. D. Meade, *Photonic Crystals: Molding the Flow of Light*, 2nd ed., Princeton University Press, Princeton, **2008**.
[105] G. R. Fowles, *Introduction to Modern Optics*, 2nd ed., Dover, New York, **1989**.
[106] L. D. Bonifacio, B. V. Lotsch, D. P. Puzzo, F. Scotognella, G. A. Ozin, *Adv. Mater.* **2009**, *21*, 1641.
[107] Y. Lu, H. Xia, G. Zhang, C. Wu, *J. Mater. Chem.* **2009**, *19*, 5952.
[108] A. Arsenault, F. Fleischhaker, G. von Freymann, V. Kitaev, H. Miguez, A. Mihi, N. Tetreault, E. Vekris, I. Manners, S. Aitchison, D. Perovic, G. A. Ozin, *Adv. Mater.* **2006**, *18*, 2779.
[109] P. A. Rundquist, P. Photinos, S. Jagannathan, S. A. Asher, *J. Chem. Phys.* **1989**, *91*, 4932.
[110] S. A. Asher, J. Holtz, L. Liu, Z. Wu, *J. Am. Chem. Soc.* **1994**, *116*, 4997.
[111] Y. J. Lee, P. V. Braun, *Adv. Mater.* **2003**, *15*, 563.
[112] H. Saito, Y. Takeoka, M. Watanabe, *Chem. Commun.* **2003**, 2126.
[113] G. Pan, R. Kesavamoorthy, S. A. Asher, *Phys. Rev. Lett.* **1997**, *78*, 3860.
[114] R. Kesavamoorthy, M. S. Super, S. A. Asher, *J. Appl. Phys.* **1992**, *71*, 1116.
[115] J. D. Debord, L. A. Lyon, *J. Phys. Chem. B* **2000**, *104*, 6327.
[116] Z. B. Hu, X. H. Lu, J. Gao, *Adv. Mater.* **2001**, *13*, 1708.
[117] Y. Takeoka, M. Watanabe, *Langmuir* **2003**, *19*, 9104.
[118] M. Kumoda, M. Watanabe, Y. Takeoka, *Langmuir* **2006**, *22*, 4403.
[119] M. Honda, T. Seki, Y. Takeoka, *Adv. Mater.* **2009**, *21*, 1801.
[120] K. Ueno, K. Matsubara, M. Watanabe, Y. Takeoka, *Adv. Mater.* **2007**, *19*, 2807.
[121] K. Matsubara, M. Watanabe, Y. Takeoka, *Angew. Chem.* **2007**, *119*, 1718; *Angew. Chem. Int. Ed.* **2007**, *46*, 1688.
[122] J. H. Kang, J. H. Moon, S. K. Lee, S. G. Park, S. G. Jang, S. Yang, S. M. Yang, *Adv. Mater.* **2008**, *20*, 3061.
[123] N. Tétreault, H. Miguez, S. M. Yang, V. Kitaev, G. A. Ozin, *Adv. Mater.* **2003**, *15*, 1167.
[124] J. H. Holtz, J. S. W. Holtz, C. H. Munro, S. A. Asher, *Anal. Chem.* **1998**, *70*, 780.
[125] C. E. Reese, S. A. Asher, *Anal. Chem.* **2003**, *75*, 3915.
[126] S. A. Asher, A. C. Sharma, A. V. Goponenko, M. M. Ward, *Anal. Chem.* **2003**, *75*, 1676.
[127] K. Lee, S. A. Asher, *J. Am. Chem. Soc.* **2000**, *122*, 9534.
[128] A. C. Sharma, T. Jana, R. Kesavamoorthy, L. J. Shi, M. A. Virji, D. N. Finegold, S. A. Asher, *J. Am. Chem. Soc.* **2004**, *126*, 2971.
[129] X. Xu, A. V. Goponenko, S. A. Asher, *J. Am. Chem. Soc.* **2008**, *130*, 3113.

[130] S. Shinohara, T. Seki, T. Sakai, R. Yoshida, Y. Takeoka, *Angew. Chem.* **2008**, *120*, 9179; *Angew. Chem. Int. Ed.* **2008**, *47*, 9039.
[131] S. Shinohara, T. Seki, T. Sakai, R. Yoshida, Y. Takeoka, *Chem. Commun.* **2008**, 4735.
[132] C. F. Blanford, R. C. Schroden, M. Al-Daous, A. Stein, *Adv. Mater.* **2001**, *13*, 26.
[133] V. N. Bogomolov, S. V. Gaponenko, I. N. Germanenko, A. M. Kapitonov, E. P. Petrov, N. V. Gaponenko, A. V. Prokofiev, A. N. Ponyavina, N. I. Silvanovich, S. M. Samoilovich, *Phys. Rev. E* **1997**, *55*, 7619.
[134] S. Y. Choi, M. Mamak, G. von Freymann, N. Chopra, G. A. Ozin, *Nano Lett.* **2006**, *6*, 2456.
[135] M. C. Fuertes, F. J. Lopez-Alcaraz, M. C. Marchi, H. E. Troiani, V. Luca, H. Miguez, G. J. A. A. Soler-Illia, *Adv. Funct. Mater.* **2007**, *17*, 1247.
[136] S. Colodrero, M. Ocana, H. Miguez, *Langmuir* **2008**, *24*, 4430.
[137] S. Colodrero, M. Ocana, A. R. Gonzalez-Elipe, H. Miguez, *Langmuir* **2008**, *24*, 9135.
[138] J. Kobler, B. V. Lotsch, G. A. Ozin, T. Bein, *ACS Nano* **2009**, *3*, 1669.
[139] M. J. Sailor, J. R. Link, *Chem. Commun.* **2005**, 1375.
[140] P. A. Snow, E. K. Squire, P. S. J. Russell, L. T. Canham, *J. Appl. Phys.* **1999**, *86*, 1781.
[141] S. Chan, S. R. Horner, P. M. Fauchet, B. L. Miller, *J. Am. Chem. Soc.* **2001**, *123*, 11797.
[142] M. Karaman, S. E. Kooi, K. K. Gleason, *Chem. Mater.* **2008**, *20*, 2262.
[143] J. M. Jethmalani, W. T. Ford, *Chem. Mater.* **1996**, *8*, 2138.
[144] S. H. Foulger, P. Jiang, A. C. Lattam, D. W. Smith, J. Ballato, *Langmuir* **2001**, *17*, 6023.
[145] H. Fudouzi, T. Sawada, *Langmuir* **2006**, *22*, 1365.
[146] S. H. Foulger, P. Jiang, A. Lattam, D. W. Smith, J. Ballato, D. E. Dausch, S. Grego, B. R. Stoner, *Adv. Mater.* **2003**, *15*, 685.
[147] M. Kamenjicki Maurer, I. K. Lednev, A. Mikhonin, R. Kesavamoorthy, S. A. Asher, *Adv. Funct. Mater.* **2003**, *13*, 774.
[148] Z. Z. Gu, S. Hayami, Q. B. Meng, T. Iyoda, A. Fujishima, O. Sato, *J. Am. Chem. Soc.* **2000**, *122*, 10730.
[149] Z. Z. Gu, T. Iyoda, A. Fujishima, O. Sato, *Adv. Mater.* **2001**, *13*, 1295.
[150] S. Kubo, Z. Z. Gu, K. Takahashi, Y. Ohko, O. Sato, A. Fujishima, *J. Am. Chem. Soc.* **2002**, *124*, 10950.
[151] S. Kubo, Z. Z. Gu, K. Takahashi, A. Fujishima, H. Segawa, O. Sato, *J. Am. Chem. Soc.* **2004**, *126*, 8314.
[152] Z.-Y. Xie, L.-G. Sun, G.-Z. Han, Z.-Z. Gu, *Adv. Mater.* **2008**, *20*, 3601.
[153] R. Wilk, N. Vieweg, O. Kopschinski, M. Koch, *Opt. Express* **2009**, *17*, 7377.
[154] J. Arriaga, L. Dobrzynski, B. Djafari-Rouhani, *J. Appl. Phys.* **2008**, *104*, 063108.
[155] V. A. Tolmachev, T. S. Perova, S. A. Grudinkin, V. A. Melnikov, E. V. Astrova, Y. A. Zharova, *Appl. Phys. Lett.* **2007**, *90*, 011908.
[156] M. Haurylau, S. P. Anderson, K. L. Marshall, P. M. Fauchet, *Appl. Phys. Lett.* **2006**, *88*, 061103.
[157] M. H. Song, B. Park, S. Nishimura, T. Toyooka, I. J. Chung, Y. Takanishi, K. Ishikawa, H. Takezoe, *Adv. Funct. Mater.* **2006**, *16*, 1793.
[158] B. Maune, M. Loncar, J. Witzens, M. Hochberg, T. Baehr-Jones, D. Psaltis, A. Scherer, Y. Qiu, *Appl. Phys. Lett.* **2004**, *85*, 360.
[159] Y. Shimoda, M. Ozaki, K. Yoshino, *Appl. Phys. Lett.* **2001**, *79*, 3627.
[160] M. Ozaki, Y. Shimoda, M. Kasano, K. Yoshino, *Adv. Mater.* **2002**, *14*, 514.
[161] K. Busch, S. John, *Phys. Rev. Lett.* **1999**, *83*, 967.
[162] A. C. Arsenault, D. P. Puzzo, I. Manners, G. A. Ozin, *Nat. Photonics* **2007**, *1*, 468.
[163] A. C. Arsenault, H. Miguez, V. Kitaev, G. A. Ozin, I. Manners, *Adv. Mater.* **2003**, *15*, 503.
[164] D. P. Puzzo, A. C. Arsenault, I. Manners, G. A. Ozin, *Angew. Chem.* **2009**, *121*, 961; *Angew. Chem. Int. Ed.* **2009**, *48*, 943.
[165] L. Xu, J. Wang, Y. Song, L. Jiang, *Chem. Mater.* **2008**, *20*, 3554.
[166] K. Ueno, J. Sakamoto, Y. Takeoka, M. Watanabe, *J. Mater. Chem.* **2009**, *19*, 4778.
[167] Y. Saado, M. Golosovsky, D. Davidov, A. Frenkel, *Phys. Rev. B* **2002**, *66*, 195108.
[168] S. Sacanna, A. P. Philipse, *Langmuir* **2006**, *22*, 10209.
[169] Z. Cun, C. Liangshui, X. Hua, G. Zhongze, *Macromol. Rapid Commun.* **2009**, *30*, 1945.
[170] J. Ge, Y. Yin, *J. Mater. Chem.* **2008**, *18*, 5041.
[171] X. L. Xu, G. Friedman, K. D. Humfeld, S. A. Majetich, S. A. Asher, *Chem. Mater.* **2002**, *14*, 1249.
[172] X. L. Xu, G. Friedman, K. D. Humfeld, S. A. Majetich, S. A. Asher, *Adv. Mater.* **2001**, *13*, 1681.
[173] G. M. Whitesides, M. Boncheva, *Proc. Natl. Acad. Sci. USA* **2002**, *99*, 4769.
[174] F. Leal Calderon, T. Stora, O. Mondain Monval, P. Poulin, J. Bibette, *Phys. Rev. Lett.* **1994**, *72*, 2959.
[175] J. Bibette, *J. Magn. Magn. Mater.* **1993**, *122*, 37.
[176] J. Ge, Y. Hu, M. Biasini, W. P. Beyermann, Y. Yin, *Angew. Chem.* **2007**, *119*, 4420; *Angew. Chem. Int. Ed.* **2007**, *46*, 4342.
[177] J. Ge, Y. Yin, *Adv. Mater.* **2008**, *20*, 3485.
[178] J. Ge, L. He, J. Goebl, Y. Yin, *J. Am. Chem. Soc.* **2009**, *131*, 3484.
[179] J. Ge, H. Lee, L. He, J. Kim, Z. Lu, H. Kim, J. Goebl, S. Kwon, Y. Yin, *J. Am. Chem. Soc.* **2009**, *131*, 15687.
[180] H. Kim, J. Ge, J. Kim, S.-E. Choi, H. Lee, H. Lee, W. Park, Y. Yin, S. Kwon, *Nat. Photonics* **2009**, *3*, 534.
[181] J. Ren, S. Song, A. Lopez-Valdivieso, J. Shen, S. Lu, *J. Colloid Interface Sci.* **2001**, *238*, 279.
[182] S. Song, C. Peng, *J. Dispersion Sci. Technol.* **2005**, *26*, 197.
[183] G. S. Roberts, R. Sanchez, R. Kemp, T. Wood, P. Bartlett, *Langmuir* **2008**, *24*, 6530.
[184] M. F. Hsu, E. R. Dufresne, D. A. Weitz, *Langmuir* **2005**, *21*, 4881.
[185] W. H. Briscoe, R. G. Horn, *Langmuir* **2002**, *18*, 3945.
[186] S. K. Sainis, V. Germain, C. O. Mejean, E. R. Dufresne, *Langmuir* **2008**, *24*, 1160.
[187] B. Gates, Y. Xia, *Adv. Mater.* **2001**, *13*, 1605.
[188] X. L. Xu, S. A. Majetich, S. A. Asher, *J. Am. Chem. Soc.* **2002**, *124*, 13864.
[189] M. Qi, E. Lidorikis, P. T. Rakich, S. G. Johnson, J. D. Joannopoulos, E. P. Ippen, H. I. Smith, *Nature* **2004**, *429*, 538.
[190] M. Deubel, G. von Freymann, M. Wegener, S. Pereira, K. Busch, C. M. Soukoulis, *Nat. Mater.* **2004**, *3*, 444.
[191] K. Aoki, H. T. Miyazaki, H. Hirayama, K. Inoshita, T. Baba, K. Sakoda, N. Shinya, Y. Aoyagi, *Nat. Mater.* **2003**, *2*, 117.
[192] F. Garcia-Santamaria, H. T. Miyazaki, A. Urquia, M. Ibisate, M. Belmonte, N. Shinya, F. Meseguer, C. Lopez, *Adv. Mater.* **2002**, *14*, 1144.
[193] R. Ozaki, T. Matsui, M. Ozaki, K. Yoshino, *Jpn. J. Appl. Phys.* **2002**, *41*, L1482.
[194] R. Ozaki, T. Matsui, M. Ozaki, K. Yoshino, *Appl. Phys. Lett.* **2003**, *82*, 3593.
[195] R. Ozaki, Y. Matsuhisa, M. Ozaki, K. Yoshino, *Appl. Phys. Lett.* **2004**, *84*, 1844.
[196] N. Tétreault, A. C. Arsenault, A. Mihi, S. Wong, V. Kitaev, I. Manners, H. Miguez, G. A. Ozin, *Adv. Mater.* **2005**, *17*, 1912.
[197] F. Fleischhaker, A. C. Arsenault, Z. Wang, V. Kitaev, F. C. Peiris, G. von Freymann, I. Manners, R. Zentel, G. A. Ozin, *Adv. Mater.* **2005**, *17*, 2455.
[198] K. U. Jeong, J. H. Jang, C. Y. Koh, M. J. Graham, K. Y. Jin, S. J. Park, C. Nah, M. H. Lee, S. Z. D. Cheng, E. L. Thomas, *J. Mater. Chem.* **2009**, *19*, 1956.
[199] Z. M. Rittersma, *Sens. Actuators A* **2002**, *96*, 196.

[200] E. T. Tian, J. X. Wang, Y. M. Zheng, Y. L. Song, L. Jiang, D. B. Zhu, *J. Mater. Chem.* **2008**, *18*, 1116.
[201] Y. J. Lee, S. A. Pruzinsky, P. V. Braun, *Langmuir* **2004**, *20*, 3096.
[202] V. L. Alexeev, A. C. Sharma, A. V. Goponenko, S. Das, I. K. Lednev, C. S. Wilcox, D. N. Finegold, S. A. Asher, *Anal. Chem.* **2003**, *75*, 2316.
[203] M. Ben-Moshe, V. L. Alexeev, S. A. Asher, *Anal. Chem.* **2006**, *78*, 5149.
[204] S. A. Asher, V. L. Alexeev, A. V. Goponenko, A. C. Sharma, I. K. Lednev, C. S. Wilcox, D. N. Finegold, *J. Am. Chem. Soc.* **2003**, *125*, 3322.
[205] J. P. Walker, S. A. Asher, *Anal. Chem.* **2005**, *77*, 1596.
[206] Y.-J. Zhao, X.-W. Zhao, J. Hu, J. Li, W.-Y. Xu, Z.-Z. Gu, *Angew. Chem.* **2009**, *121*, 7486; *Angew. Chem. Int. Ed.* **2009**, *48*, 7350.
[207] C. Sun, X.-W. Zhao, Y.-J. Zhao, R. Zhu, Z.-Z. Gu, *Small* **2008**, *4*, 592.
[208] Y. J. Zhao, X. W. Zhao, J. Hu, M. Xu, W. J. Zhao, L. G. Sun, C. Zhu, H. Xu, Z. Z. Gu, *Adv. Mater.* **2009**, *21*, 569.
[209] J. Hu, X.-W. Zhao, Y.-J. Zhao, J. Li, W.-Y. Xu, Z.-Y. Wen, M. Xu, Z.-Z. Gu, *J. Mater. Chem.* **2009**, *19*, 5730.
[210] M. Li, F. He, Q. Liao, J. Liu, L. Xu, L. Jiang, Y. Song, S. Wang, D. Zhu, *Angew. Chem.* **2008**, *120*, 7368; *Angew. Chem. Int. Ed.* **2008**, *47*, 7258.
[211] B. V. Lotsch, C. B. Knobbe, G. A. Ozin, *Small* **2009**, *5*, 1498.
[212] A. C. Arsenault, T. J. Clark, G. Von Freymann, L. Cademartiri, R. Sapienza, J. Bertolotti, E. Vekris, S. Wong, V. Kitaev, I. Manners, R. Z. Wang, S. John, D. Wiersma, G. A. Ozin, *Nat. Mater.* **2006**, *5*, 179.
[213] G. A. Ozin, A. C. Arsenault, *Mater. Today* **2008**, *11*, 44.
[214] J. Park, J. Moon, H. Shin, D. Wang, M. Park, *J. Colloid Interface Sci.* **2006**, *298*, 713.
[215] D. Allard, B. Lange, F. Fleischhaker, R. Zentel, M. Wulf, *Soft Mater.* **2005**, *3*, 121.
[216] J. G. McGrath, R. D. Bock, J. M. Cathcart, L. A. Lyon, *Chem. Mater.* **2007**, *19*, 1584.
[217] S. E. Chung, W. Park, H. Park, K. Yu, N. Park, S. Kwon, *Appl. Phys. Lett.* **2007**, *91*, 041106.
[218] S. E. Chung, W. Park, S. Shin, S. A. Lee, S. Kwon, *Nat. Mater.* **2008**, *7*, 581.
[219] O. Sato, S. Kubo, Z.-Z. Gu, *Acc. Chem. Res.* **2009**, *42*, 1.
[220] Y. Kang, J. J. Walish, T. Gorishnyy, E. L. Thomas, *Nat. Mater.* **2007**, *6*, 957.
[221] H. Fudouzi, Y. N. Xia, *Langmuir* **2003**, *19*, 9653.
[222] H. Fudouzi, Y. N. Xia, *Adv. Mater.* **2003**, *15*, 892.
[223] P. Jiang, D. W. Smith, J. M. Ballato, S. H. Foulger, *Adv. Mater.* **2005**, *17*, 179.
[224] J. Ge, J. Goebl, L. He, Z. Lu, Y. Yin, *Adv. Mater.* **2009**, *21*, 4259.
[225] A. Toyotama, T. Kanai, T. Sawada, J. Yamanaka, K. Ito, K. Kitamura, *Langmuir* **2005**, *21*, 10268.
[226] Q. Cao, Z.-T. Zhu, M. G. Lemaitre, M.-G. Xia, M. Shim, J. A. Rogers, *Appl. Phys. Lett.* **2006**, *88*, 113511.
[227] S. Ju, A. Facchetti, Y. Xuan, J. Liu, F. Ishikawa, P. Ye, C. Zhou, T. J. Marks, D. B. Janes, *Nat. Nanotechnol.* **2007**, *2*, 378.
[228] X. Li, Y. Zhu, W. Cai, M. Borysiak, B. Han, D. Chen, R. D. Piner, L. Colombo, R. S. Ruoff, *Nano Lett.* **2009**, *9*, 4359.

